An Assessment of the Cumulative Impacts of Floating Offshore Wind Farms

Agreement Number C0210404

Prepared for

Ocean Protection Council
715 P St., 20th Floor
Sacramento, CA 95814

Prepared by

200 Washington Street
Suite 201
Santa Cruz, CA 95060

December 31, 2021

CONTENTS

LIST OF FIGURES

LIST OF TABLES

ACRONYMS AND ABBREVIATIONS

BOEM	Bureau of Ocean Energy Management
BEUTI	Biologically Effective Upwelling Transport Index
CCS	California Current System
CEC	California Energy Commission
CFD	Computational Fluid Dynamics
COAMPS	Coupled Ocean / Atmosphere Mesoscale Prediction System
CUTI	Coastal Upwelling Transport Index
ECMWF	European Center for Medium Range Weather Forecasts
ENSO	El Niño Southern Oscillation
ERA5	ECMWF Reanalysis v5
MLD	Mixed Layer Depth
NMFS	National Marine Fisheries Service
OISST	Optimum Interpolation Sea Surface Temperature
OPC	Ocean Protection Council
ROMS	Regional Ocean Modeling System
SODA	Simple Ocean Data Assimilation
SOWFA	Simulator of Wind Farm Applications
SST	Sea Surface Temperature
WC12	West Coast 12
WC15	West Coast 15
WFP	Wind Farm Parameterization
WRF	Weather Research and Forecasting

EXECUTIVE SUMMARY

In California offshore waters, sustained northwesterly winds have been identified as a key energy resource which could contribute substantially to California's renewable energy mandate (Senate Bill 100). However, the development of large-scale offshore wind energy projects has the potential to reduce the wind stress at the sea surface, which could have local and/or regional implications on California wind-driven upwelling, nutrient delivery, and ecosystem dynamics. Under a current project funded by the California Energy Commission (CEC) (EPC-19-009), Integral Consulting Inc. (Integral) is evaluating potential changes in California coastal upwelling from offshore wind project development over a variety of environmental conditions, device characteristics, and wind farm configurations.

The work described here under Ocean Protection Council (OPC) funding accelerated the timeline upon which results from the CEC project are reported for the existing coupled numerical atmospheric-ocean circulation models, without (baseline) and with simulated turbines. Described in this report is a comparison of upwelling effects resulting from the installation of wind turbines offshore of Morro Bay, Diablo Canyon and Humboldt using operational upwelling metrics for physical transport and nutrient delivery. Modest changes to wind speeds are found in the lee of wind farms, which leads to a decrease in upwelled physical volume transport and resulting nutrient supply to the coastal zone in the vicinity of the Morro Bay and Diablo Canyon call areas. While changes are also observed near the Humboldt call area, they are substantially smaller than those seen near Morro Bay. Since the effect of this decrease on the ecosystem was not evaluated in this study, no conclusions on ecosystem effects can be drawn from the modeled physical changes.

1 INTRODUCTION

In California offshore waters, sustained northwesterly winds have been identified as a key energy resource, with the offshore wind resource potential estimated at 112 gigawatts (Musial et al., 2016), which could contribute substantially to California's renewable energy mandate (Senate Bill [SB] 100). The key advantage of offshore wind over its land-based counterpart is that the offshore wind resource is far more consistent, reliable, and energetic, with little of the topographic and small-scale variability typically observed over land. It is believed that floating offshore wind technologies could reach capacity factors of more than 70%, and the levelized cost of energy of floating offshore wind devices is projected to decrease by as much as 53% by 2050 (Wiser et al., 2016), making offshore wind a viable energy source. However, grid connectivity and lack of understanding of potential environmental impacts are current barriers to offshore wind that require further investigation and mitigation.

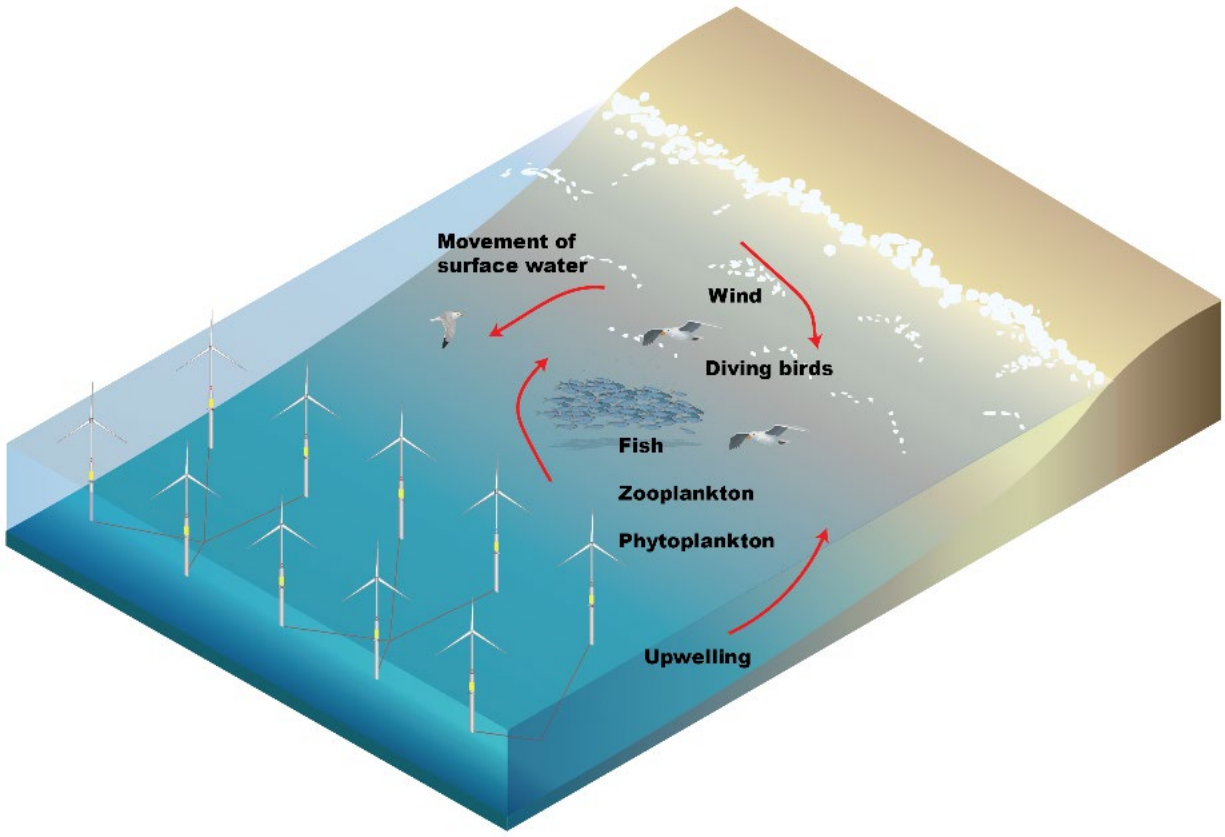

Figure 1. Upwelling dynamics around an offshore wind farm.

Wind-driven upwelling is responsible for much of the primary productivity that sustains one of the richest ecosystems on the planet (Xiu et al., 2018). Wind-driven upwelling along the California coast is forced two ways (Figure 1): first, northwesterly winds drive offshore Ekman transport near the coast, which produces coastal divergence and consequently, upwelling of deep, nutrient-rich waters in a band adjacent to the coast whose width is approximately the baroclinic Rossby radius of deformation (in the range of 10-20 kilometers at these latitudes). Second, wind stress curl (horizontal gradients in the wind) drives divergent flow near the ocean's surface and consequently, upwelling (Ekman suction) that can extend farther offshore than that driven by coastal divergence (Rykaczewski & Checkley, 2007; Checkley & Barth, 2009). Thus, an offshore wind farm project equal to an approximate lease block area of 20x20 km is on the order of spatial scales at which rotational effects such as upwelling occurs can be impacted. The development of large-scale offshore wind energy projects has the potential to reduce the wind stress at the sea surface, which could have local and/or regional implications on California wind-driven upwelling, nutrient delivery, and ecosystem dynamics. It is therefore necessary to investigate the effects of large-scale wind farms on coastal upwelling in the context of historical climatology as well as climate change predictions, including a risk assessment to the ecosystem and socioeconomic impact analysis.

Three California offshore wind lease areas were originally recognized by the Bureau of Ocean Energy Management (BOEM) [Docket No. BOEM-2018-0045]—Humboldt, Morro Bay, and Diablo Canyon—where suitable offshore wind resources have been identified (Musial et al., 2016). At the time of this writing, the Diablo Canyon call area is no longer under consideration, while the size and shape of the Morro Bay call area has been modified (initially, Morro Bay 399 and now, Morro Bay 376). These sites provide essential habitat and migration routes for a variety of marine life including threatened and endangered species of birds (e.g., Marbled murrelet, Short-tailed albatross), marine mammals (e.g., Blue and Fin whale), sea turtles (Loggerhead, Leatherback, Green, and Olive Ridley), fish (e.g., Green sturgeon, salmon, and steelhead), and invertebrates (abalone). Further, these areas support commercial and recreational fishing and a maritime economy valued at approximately $22 billion (National Marine Fisheries Service [NMFS], 2018).

With the exception of the Horns Rev study (Jimenez et al., 2015) that was applied to a 21 km^2 wind farm, there have been relatively few studies that have examined wind stress reductions at the sea surface for large offshore wind farms, such as those planned offshore of California. Of particular relevance to this study are works by Duin (2019) and Huang & Hall (2015). Duin (2019) studied wind stress reductions for a large offshore wind farm in the North Sea and found that typical wind speeds 10 m above the sea surface are reduced by up to 1 m/s, with secondary effects on air temperature, relative humidity, and radiation.

Specific to California, Huang & Hall (2015) implemented an atmospheric model to a 10x10-km wind farm offshore of Bodega Bay, California. The authors implemented an open-source atmospheric model (Weather Research and Forecasting [WRF]), a version of which parameterizes extraction of wind energy by a turbine as a function of hub height, efficiency coefficient, and blade width. The authors found approximately 10% reduction in wind speeds, with reductions that extended 100 km downstream. Additionally, temperature decreases in the lower marine boundary layer were reported, accompanied by increases in humidity. The effects of these reduced wind speeds on ocean circulation were not considered by Huang & Hall (2015), and appear to be a work in progress.

There are few studies of the effects of large-scale offshore wind turbines on coastal wind-driven upwelling. Brostrom (2008) examined formation of wind stress curl-driven upwelling in a large wind farm district and found that pycnocline displacement increased as a function of wind farm length. Paskyabi & Fer (2012) studied strength of coastal upwelling and wind farm size, and reported that wakes are able to increase the magnitude of pycnocline displacements. Paskyabi (2015) investigated two empirical wake models, including a model of change in the structure of coastal upwelling and stratification caused by a large wind farm. These studies focused on European wind farms, which are often in shallower water than is likely to be the case in California.

Recent advances in high-performance computing allow for the application of regional scale numerical circulation models to yield insights into the various driving forces and sensitivities of upwelling dynamics to these forcing mechanisms (e.g., Veneziani et al., 2009). More recently, physical and coupled biogeochemical models have been used to examine the sensitivity of ocean physics and phytoplankton production in the California Current System (CCS) to forcing mechanisms (e.g., Jacox et al., 2015, 2016) and account for multiple phytoplankton species including their predation by zooplankton (Goebel et al., 2010; Raghukumar et al., 2015; Fiechter et al., 2018). The use of the aforementioned atmospheric and ocean circulation models therefore represent mature and powerful numerical tools by which to evaluate the potential effects of offshore wind farms on coastal upwelling, the subject of this report.

In this study, a one-way coupled atmosphere-ocean model is applied to evaluate changes to upwelling following the introduction of wind farms at Humboldt, Morro Bay, and Diablo Canyon, all of which were part of the original set of call areas at the time this study commenced. Since then, the Diablo Canyon call area will likely not be considered for future wind farm development. Nevertheless, these results can be considered to represent an upper-bound on potential upwelling effects of offshore wind, and consistent with the project design envelope approach favored in drafting offshore wind construction and operation plans.

2 APPROACH

Here, as a first step to undertaking a complete environmental risk assessment, an atmosphere-ocean model is implemented that evaluates the effect of wind stress reduction on ocean circulation. Turbines at full build-out are implemented in the Humboldt, Morro Bay, and Diablo Canyon call areas, and the effect of wind stress reduction on coastal upwelling is investigated. The analysis then proceeds to determine potential changes in coastal upwelling due to offshore wind project development over a 13-year period (1988-2000) that encompasses a variety of environmental conditions.

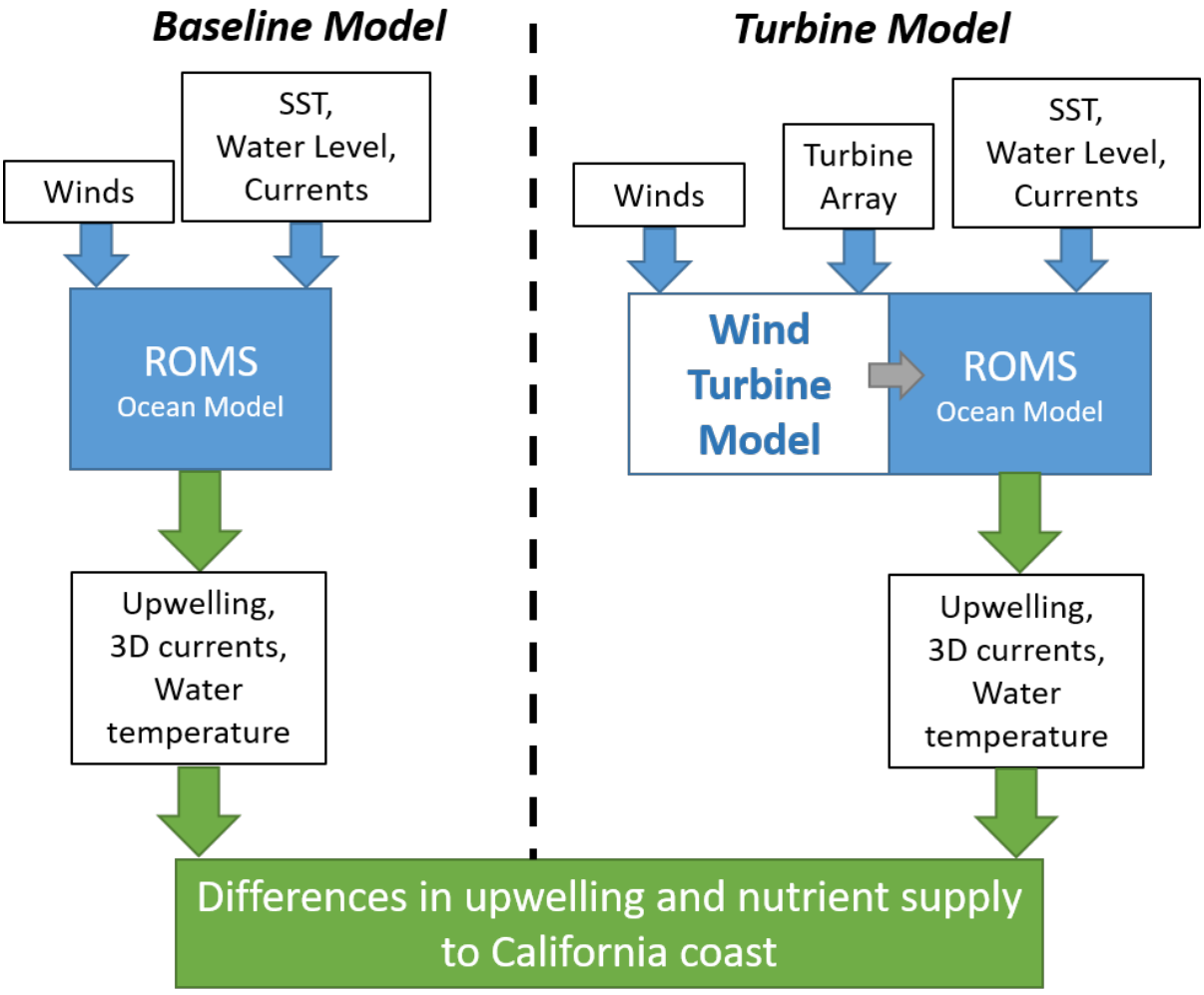

Figure 2. Flowchart of approach to evaluate changes to upwelling following the introduction of an offshore wind farm.

The modeling study is enabled using a high-resolution wind model, WRF, which accounts for turbine-turbine and wake-turbine interactions and thereby provides an accurate assessment of the wind field around a wind farm (e.g., Churchfield et al., 2012).

As shown in Figure 2, the approach begins with the evaluation of WRF wind fields in the absence and presence of wind turbines. Wind fields are then coupled to a regional ocean circulation model, Regional Ocean Modeling System (ROMS) with higher resolution grids nested around the wind farms. This nesting allows for the computation of upwelling indices of relevance to primary production, and potential changes in these indices (Jacox et al., 2018). In turn, the computation of upwelling indices will allow for the eventual inference of impacts on primary production and fisheries.

Below are described the specifics of each model and the coupling methodology.

2.1 WEATHER RESEARCH AND FORECASTING (WRF) WIND MODEL

The open-source WRF model with the wind farm parameterization (WFP) module is applied to examine changes to wind fields following the introduction of offshore wind projects off California. The WRF-WFP model (Fitch et al., 2012) represents wind turbines as a momentum sink and turbulence source, and allows for the specification of turbine parameters such as hub height, rotor diameter, power curve, and thrust coefficients (Lee & Lundquist, 2017). By allowing for wind farm parameterization within an established and validated operational weather model, WRF-WFP has been utilized in a number of studies to evaluate the effects of wind farms on mesoscale weather patterns. For example, Eriksson et al. (2015) compared WRF-WFP with large eddy simulations (LES) of wind farms and found that while power production was better estimated by the LES, the two methods showed similar wake expansion. Jimenez et al. (2015) conducted an observational and modeling study at the Horns Rev offshore wind farm (Denmark) and concluded that the WRF-WFP model qualitatively reproduced wind farm power deficits.

In this study, the WRF-WFP model is applied to the Eastern Pacific region, with a higher resolution nest that contains the continental shelf along the California coast. Simulated offshore wind farms are placed within three call areas, each approximately 100 x100 km, and located offshore of Humboldt, Morro Bay, and Diablo Canyon. In this assessment, each nominated lease block is fully 'built-up', with turbines occupying the entire call area. Figure 3 shows the model grid extents, topography and a vertical section of the modeled wind turbines overlaid on WRF vertical levels between the surface and 1200 m above the sea surface.

The WRF model is configured to use two levels of horizontal discretization, with each model grid set up using a Mercator projection. The coarser, outer nest consists of 150 x 144 cells in the latitudinal and longitudinal directions, respectively, with Δx = 15 km. The inner, finer nest consists of 426 x 516 cells and Δx = 3 km. Each nest has 61 terrain-following vertical levels that

span from the sea surface to approximately 3.4 km height above the sea surface. The horizontal discretization values were chosen to correspond with the discretization of an accompanying ocean circulation model, and follow recommendations from Tomaszewski et al. (2020) for refinement levels of inner nest WRF simulations of wind turbines. Both the outer and inner domains are centered nominally at latitude and longitude coordinates of 39°N and 122.75°W, with the outer domain spanning longitudinal values from 136°W to 110°W, and latitudinal values from 29.5°N to 48.5°N. The inner, refined domain spans longitudinal values from 130°W to 115°W, and latitudinal values from 31.1°N to 45.25°N.

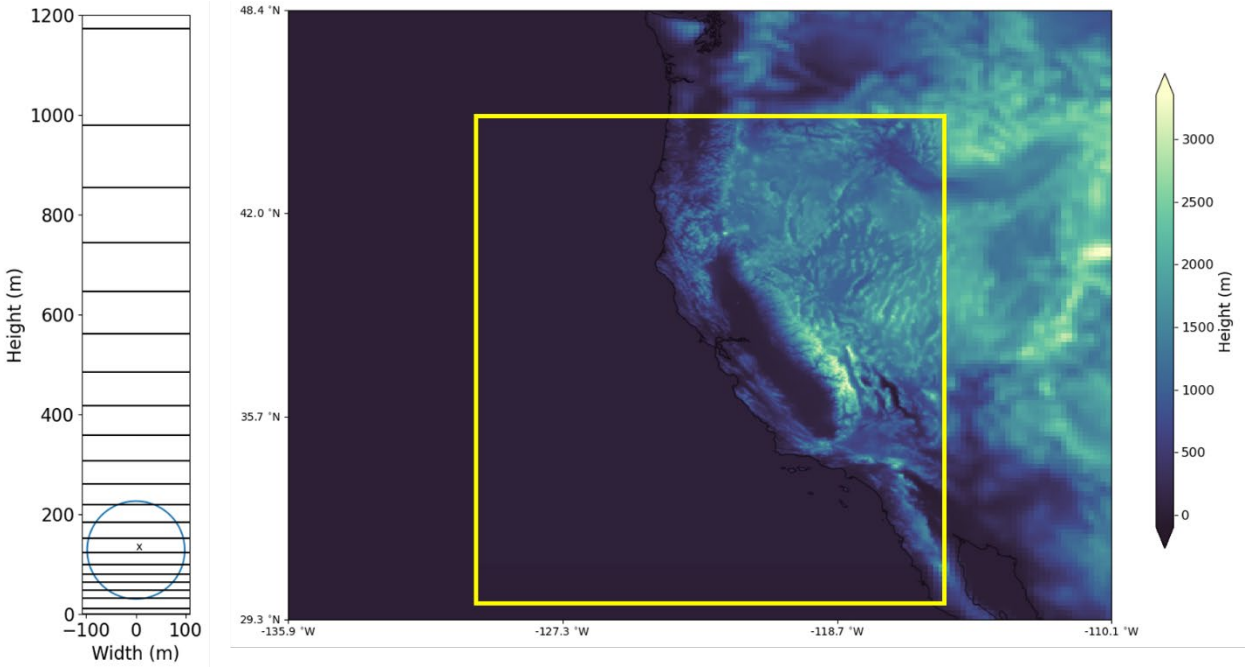

Figure 3. (Left) Vertical profile of modeled wind turbine, overlaid on a subset of the terrain-following vertical terrain levels, (right) WRF model grid extents overlaid on topography

The European Center for Medium Range Weather Forecasts (ECMWF) Reanalysis v5 (ERA5, Hersbach et al., 2018) were used to provide the pressure and surface input conditions for the WRF model. The quality-assured ERA5 boundary conditions cover the Earth on a 30 km grid and resolve the atmosphere using 137 levels from the surface to a height of 80 km. The physics parameters and boundary condition fields used in the WRF model implementation are identical to the validated model used to develop the Wind Toolkit (Optis et al., 2020), and therefore no duplicate validation effort was performed for this study.

2.2 TURBINE PARAMETERS

Turbine parameters (hub height of 128 m and diameter of 196 m, thrust and power coefficient curves) are taken from the 10 MW floating offshore turbine model described in Beiter et al. (2020) with a commercial operation date of 2022.

Turbines are placed within each call area, assuming a full project build-out, as shown in Figure 4. Water depths for the turbine locations range from 800 m to 2000 m. The locations of turbines within the Humboldt call area are identical to that reported by Severy & Garcia (2020), which consisted of 152 turbines spaced roughly 1.8 km apart (approximately 9 turbine diameters, i.e. 9D spacing). A similar (~9D) turbine spacing was applied to the Morro Bay and Diablo Canyon call areas, resulting in a total of 230 and 495 turbines in each Central Coast nominated call area, respectively.

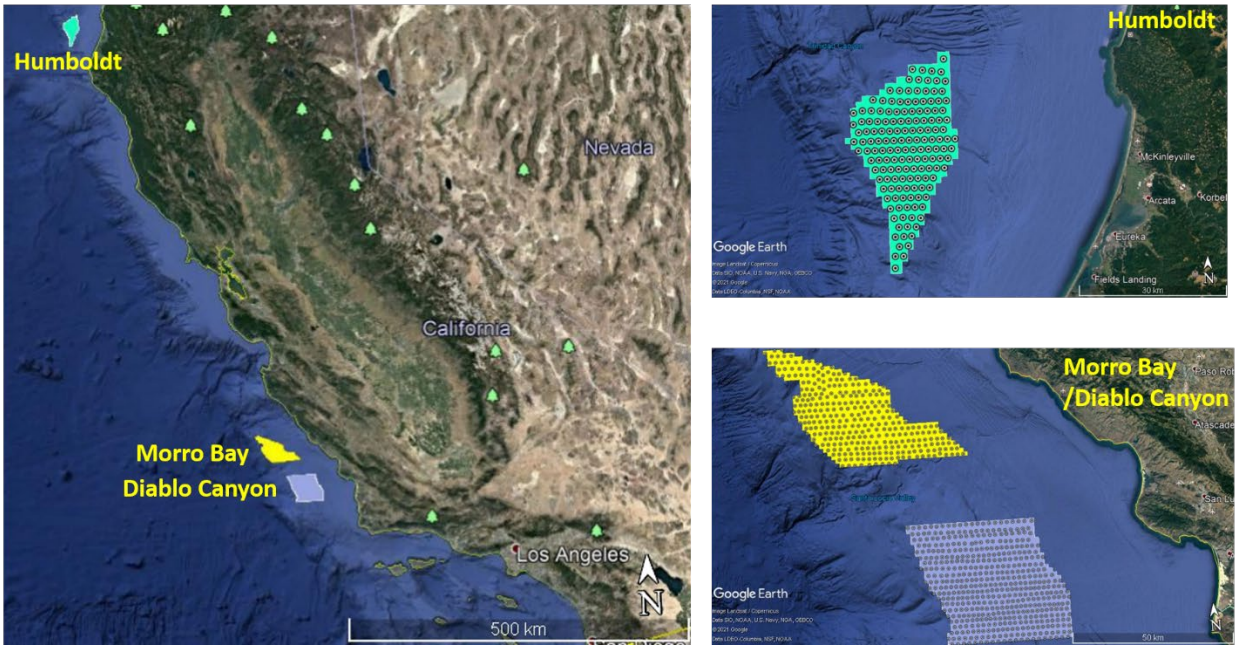

Figure 4 (Left) Overview of wind farm call areas, (top right) zoom of Humboldt call area with turbine locations, (bottom right) zoom of Morro Bay and Diablo Canyon call areas with turbine locations.

A summary of turbine parameters is provided in Table 1.

Table 1. Modeled wind turbine parameters.

Parameter	Value
Number of turbines	152 (Humboldt), 230 (Morro Bay), 495 (Diablo Canyon)
Hub height	128 m
Rotor Diameter	196 m
Power output	10 MW
Turbine spacing	1.8 km (~9D)

2.3 REGIONAL OCEAN MODELING SYSTEM (ROMS) OCEAN CIRCULATION MODEL

All ocean modeling described in this study uses ROMS (Shchepetkin & McWilliamns, 2005). ROMS is a free-surface, terrain-following, primitive equations ocean model widely used by the scientific community for a diverse range of applications (e.g., Haidvogel et al., 2000; Marchesiello et al., 2003; Peliz et al., 2003; Di Lorenzo, 2003; Dinniman et al., 2003; Budgell, 2005; Wilkin et al., 2005). The model configuration is similar to that discussed by Veneziani et al. (2009) and Neveu et al. (2016).

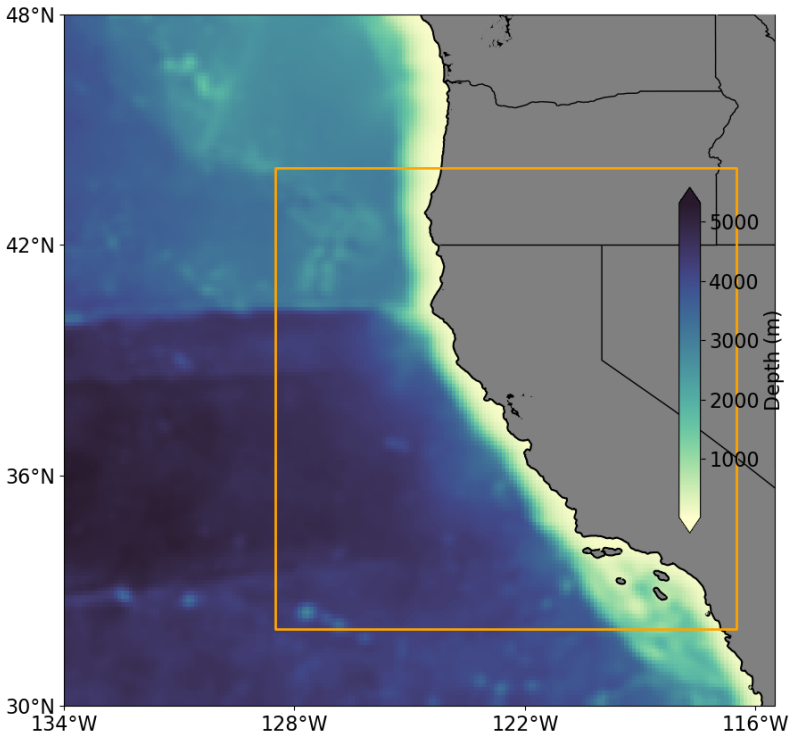

Figure 5. ROMS model bathymetry for each domain, the 10 km outer domain (WC12) and the 3 km inner domain (WC15), demarcated by the orange box.

The model consists of two domains (Figure 5): the outer domain (herein referred to as WC12) that spans from the middle of the Baja peninsula to the southern tip of Vancouver Island, and over 1000 km zonally, covering 30-48°N and 116.5-134°W, at 10 km resolution with 42 terrain-following vertical levels, while the inner domain (herein referred to as WC15) spans from 32-44°N and 116-128°W at a 3 km resolution, also with 42 terrain following vertical levels. Surface forcing fields consist of horizontal wind speeds 10 m above the sea surface, air temperature, and specific humidity 2 m above the sea surface, surface air pressure, precipitation, downward longwave radiation, and net shortwave radiation, and are derived from the WRF model (Section 2.1). The surface forcing fields for the WC12/WC15 domains consist of WRF fields from the outer/inner WRF domains, linearly interpolated onto the ROMS domains. Boundary and initial conditions for the WC12 model are derived from the data assimilative reanalysis of the WC12 model (Neveu et al., 2016), which in turn was initialized by the Simple Ocean Data Assimilation (SODA) analysis of the global upper ocean (Carton et al., 2000).

Both ROMS models (WC12 and WC15) have been utilized extensively in physical oceanographic and ecosystem studies of the California Current System, in addition to forming the basis of operational modeling at the Central California Ocean Observing System. For example, Veneziani et al. (2009) developed the model and validated the accuracy of the model in its present configuration to correctly represent circulation features. Broquet et al. (2009) implemented a data assimilation framework to improve model performance by nudging the model solution towards observations in a physically meaningful manner, while Neveu et al. (2016) compared data assimilative WC12 model solutions when assimilating various atmospheric products. Ecosystem studies using the WC12 model include those by Goebel et al. (2010) who configured a lower-trophic level ecosystem model to the physical circulation model, while Raghukumar et al. (2015) examined the impacts of data assimilation on modeled ecosystem responses. More recently, Fiechter et al. (2018) developed the 3 km WC15 nest and applied the nested WC12-WC15 model to examine the effects of alongshore variability in winds and physical circulation on modeled phytoplankton estimates. Upwelling-specific studies using the WC12 model include those by Jacox et al. (2015), who examined upwelling variability using a historical analysis of circulation of the California Current System and Lowe (2020), who used the WC12 model along with multiple high resolution nests to examine canyon-driven nearshore upwelling and the resulting effects of larval transport.

2.4 UPWELLING METRICS

For 50 years, upwelling indices (Bakun, 1973, 1975) have been used to monitor and understand coastal upwelling along the U.S. west coast and its impacts on the marine ecosystem from phytoplankton to top predators. Initially, these indices were computed using coarse resolution atmospheric pressure fields. More recent advances (Jacox et al., 2018) have allowed more accurate quantification of upwelling and downwelling (i.e., the vertical transport into or out of

the surface mixed layer) as well as nutrient fluxes associated with this transport. Specifically, two indices are routinely produced at NOAA's Southwest Fisheries Science Center: the Coastal Upwelling Transport Index (CUTI), which estimates vertical volume transport, and the Biologically Effective Upwelling Transport Index (BEUTI), which estimates vertical nitrate flux.

Here, CUTI and BEUTI are computed based on the high-resolution ocean and atmosphere model outputs described previously. Both indices are calculated for 1° latitudinal bins along the U.S. west coast (Figure 6). The cross-shore extent of upwelling captured by the indices can be varied; the analysis here is focused mainly on the 50 km zone adjacent to the coast – the most productive upwelled waters - but upwelling changes are also calculated for greater cross-shore extents (75 and 100 km). CUTI is calculated as the net transport out of a given latitudinal bin, which must be balanced by vertical transport into the surface mixed layer (i.e., upwelling). BEUTI, the vertical nitrate flux, is calculated by multiplying CUTI by the nitrate concentration at the base of the mixed layer. Since the ocean model does not explicitly represent nitrate, it is estimated from a latitude-nitrate-temperature relationship that is very robust in the CCS (capturing ~95% of the observed nitrate variance, Jacox et al., 2018).

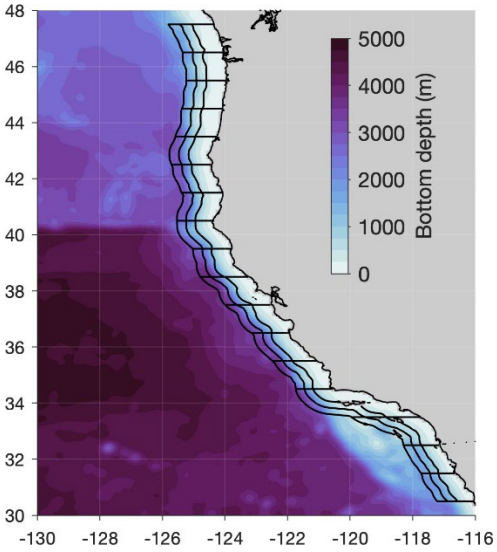

Figure 6. Regions for upwelling index locations are shown on the ROMS model grid (bottom depth in color). Contours outline 1° latitudinal bins used to calculate upwelling indices, with offshore extents of 50, 75, and 100 km.

2.5 MODEL IMPLEMENTATION

The models are run for the period between the years 1988 and 2000. The WRF models are run using online nesting, with no feedback between the inner and outer domain (i.e. model fields propagate from the outer into the inner domain, but not vice versa). The no-feedback option was chosen to eliminate artifacts at the boundaries of the inner domain. WRF model fields for

each domain are available every 3 hours, on a Mercator projection. These fields are then linearly interpolated onto the ROMS WC12/WC15 grids for use as forcing fields. WRF fields for each domain are available in the absence and presence of turbines in the Humboldt, Morro Bay, and Diablo Canyon call areas.

Once forcing fields are available, the two ocean model domains are run using offline nesting. Here, the WC12 model is first run using the outer WRF domain forcing fields (interpolated onto the WC15 grid) for the period spanning 1988-2000. Daily averaged fields are stored, and used to generate initial and boundary conditions for the WC15 model. The WC15 model is then run for the 1988-2000 time period, and model results evaluated.

3 RESULTS

3.1 ATMOSPHERIC MODEL

Here, we discuss results from the WRF model runs over a period of 13 years, covering the years 1988-2000, assuming full build-out of turbines at all three call areas (Humboldt, Morro Bay, and Diablo Canyon). The model was run without and with turbines and the differences in atmospheric circulation were compared. Atmospheric fields of particular interest were those that constitute forcing fields to an ocean circulation model, namely: horizontal winds at 10 m height, specific humidity at 2 m height, downward longwave radiation, net shortwave radiation, precipitation, and surface air temperature at 2 m height above the sea surface.

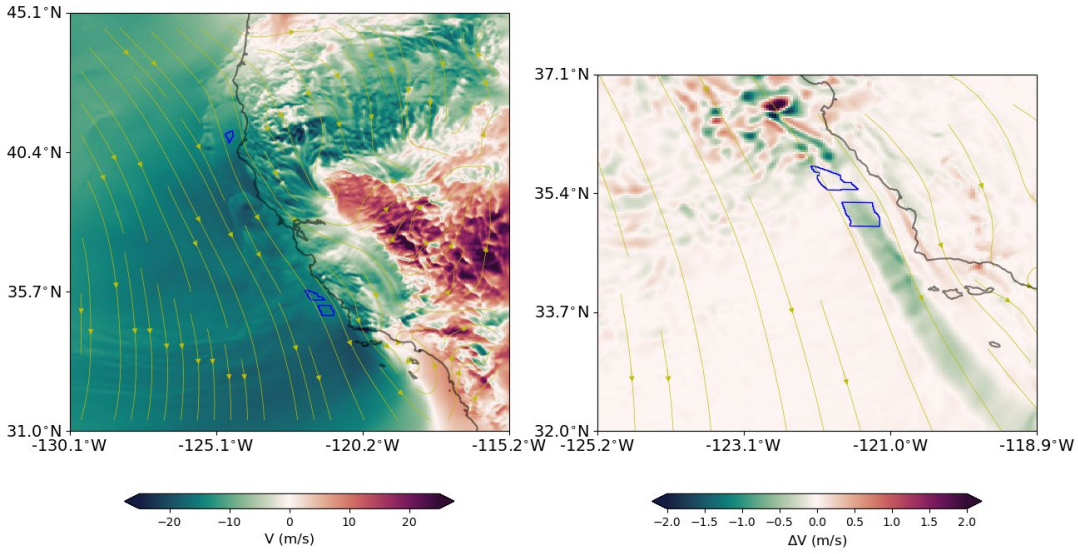

Figure 7. (Left) North-south component of hub-height velocity (V-velocity) on April 15, 2000 at 12:00:00, and, (right) difference in hub-height V-velocity, zoomed in around the Morro Bay/Diablo Canyon call area. Call areas for the Humboldt, Morro Bay and Diablo Canyon are marked by the blue outlines. Difference = without – with turbines.

Figure 7 shows an example of the approximate hub-height (127.12 m) meridional velocity (V-velocity, positive to the north) for the entire model domain, as well as a close-up of V-velocity deficit (no turbines minus turbines) for the Morro Bay and Diablo Canyon call areas at a single time instance (April 15, 2000) in the simulation. Wind speeds over land are observed to show considerable topographic variability, modulated by the Coast Ranges, central plains and the Sierra Nevada mountains. In contrast, the offshore meridional velocities are predominantly northwesterly, with wind speeds that approach 25 m/s. Significant reduction of the northwesterly winds are observed south of Point Conception which marks a distinct biogeographic boundary between Central and Southern California. The map of the meridional velocity deficit shows a marked reduction in meridional winds in the lee of the Morro Bay/Diablo Canyon call area, with the wake extending south of the Channel Islands.

Instantaneous reductions in velocity range from a maximum of 1 m/s down to 0.25 m/s or less offshore of Los Angeles. In addition to wake effects extending to the lee of the predominant wind direction, shorter-term wake effects are seen north of the call areas, presumably due to eddying of wind fields. While distinct in Figure 7, these shorter term wakes are not expected to affect coastal upwelling which requires sustained northwesterly winds on time scales of several days to weeks.

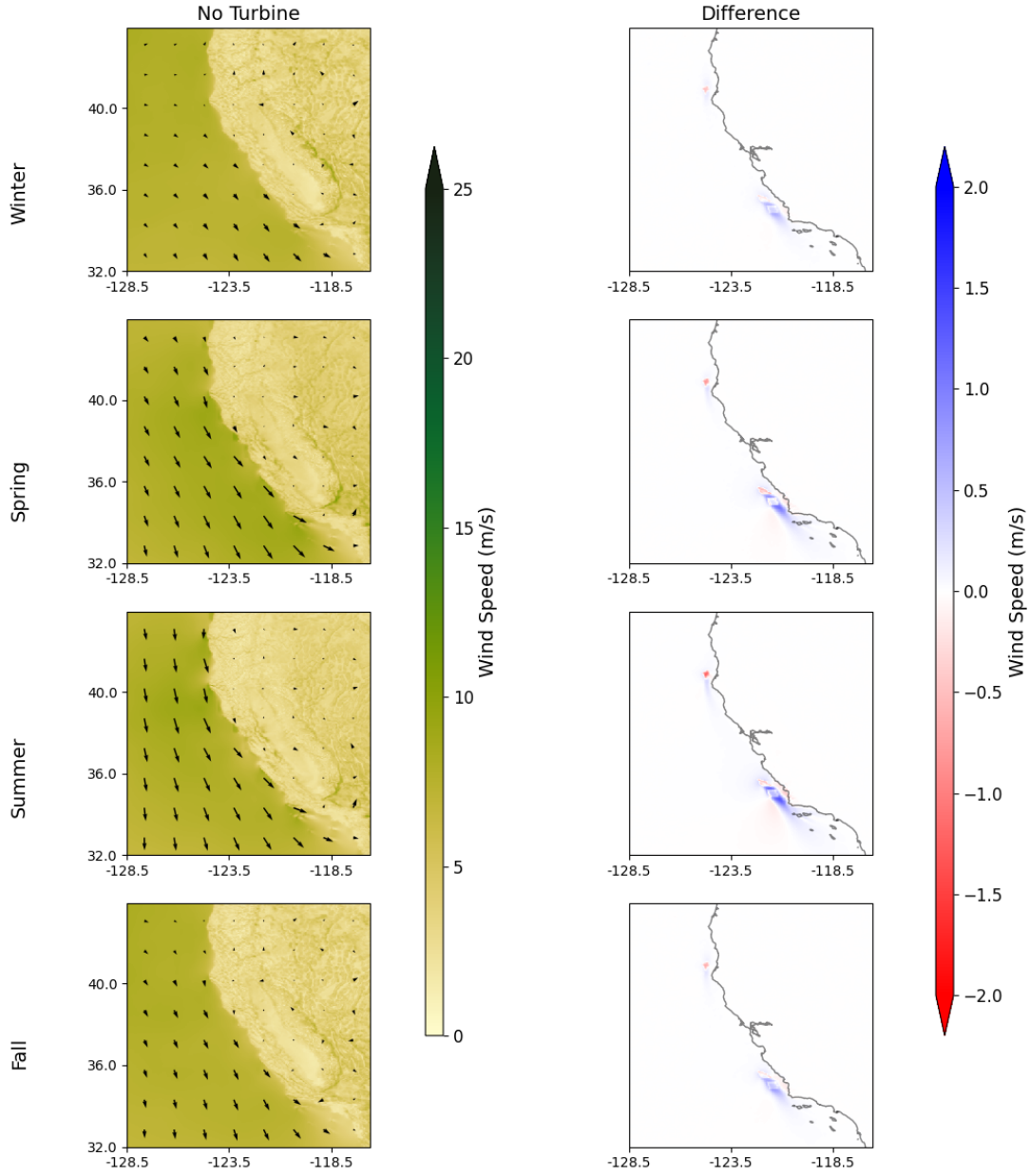

Figure 8. Seasonal variability in wind speeds in the absence and presence of simulated turbines. Difference = without – with turbines.

Figure 8 shows wind speed and direction across seasons (winter- January to March, spring- April to June, fall- July to September, winter- October to December), in the absence and presence of simulated turbines. Also shown are the differences in wind speeds (no turbines minus turbines). Sustained northwesterly winds are observed in the spring and summer months, accentuated by particularly intense winds between 10-15 m/s around headlands such as Cape Mendocino and Point Conception. Accompanied by the intensification of winds are the corresponding differences in wind speeds that approach 1 m/s (~5% reduction) within the Morro Bay/Diablo Canyon call areas. Further, the wakes induced by the simulated wind turbines, or the regional extent of wind speed reduction, is often seen to extend southward past the Channel Islands, covering an aerial extent of approximately 14,000 km^2, with a length scale of approximately 200 km (as also seen in Figure 8). Wind speeds generally trend lower as fall transitions to winter, typical of weather patterns along the California coast.

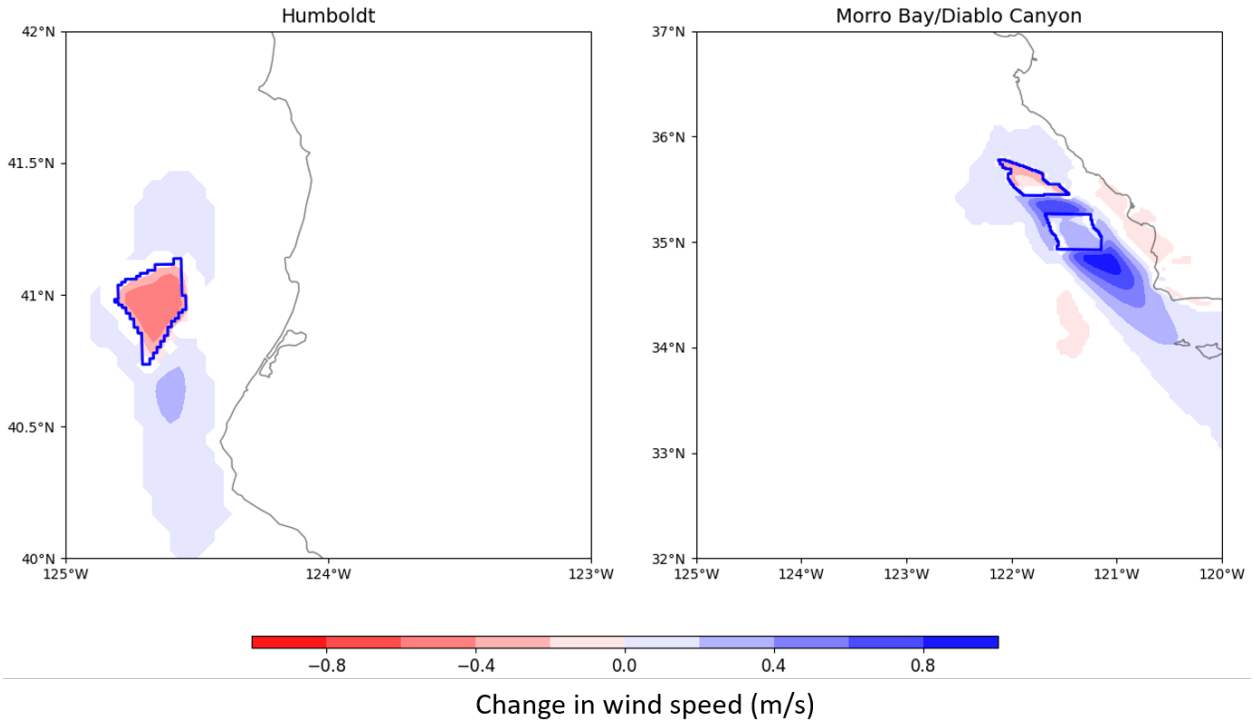

Figure 9. Spring season differences in wind speeds around the call areas. Difference = without – with turbines.

Figure 9 shows a close-up of spring season wind speed changes around each of the call areas, at 10 m height above the sea surface. The increase in wind speeds in the immediate vicinity of the call areas is readily apparent, attributed to the speed-up in wind speeds around the turbine tips (Bernoulli effect). The dependence of the increase in wind speeds on background wind speeds is also evident, wherein the increase in wind speed inside the call area is more pronounced in the presence of lower background wind speeds (such as in Humboldt), while a higher background

wind speed results in a smaller region in the call area that is subject to an increase in wind speeds.

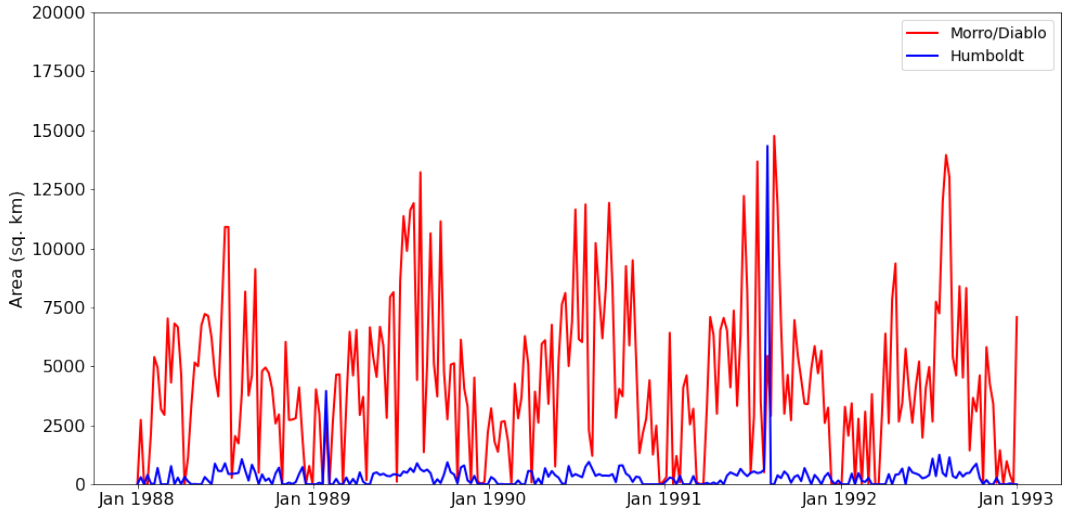

Figure 10. Area over which wind speeds are reduced by more than 0.5 m/s around the Humboldt and Morro Bay/Diablo Canyon call areas.

Given the changes in wind speeds, and due to the importance of spatial scales of wind speed reductions on coastal upwelling, the area affected by wind speed reductions at each nominated lease block was calculated over the 13 year-long WRF simulation. Figure 10 shows the area over which wind speed reductions are larger than 0.5 m/s when applied to weekly-averaged wind speeds in the absence and presence of simulated wind turbines. The largest areas affected are around the Morro Bay/Diablo Canyon sites, with areas on the order of 12,500 km^2, consistent with Figure 8 where wind speeds are observed to be largest in the summer. Also observed is a seasonal modulation of the area affected, consistent with the largest wind speeds occurring between April and September. With the exception of the large spike in May 1999 (due to wind speeds exceeding 25 m/s within the Humboldt call area), effects observed at the Humboldt site are significantly smaller than those at the Morro Bay/Diablo Canyon sites, consistent with the smaller areal footprint of the Humboldt call area.

3.2 OCEAN MODEL

Here, we discuss ROMS model runs over a period of 13 years, over the period 1988-2000, assuming full build-out of turbines at all three call areas (Humboldt, Morro Bay, and Diablo Canyon). The model was forced using WRF model output, without and with turbines, with the WRF fields interpolated onto the WC12 and WC15 ROMS grids.

Prior to comparison of modeled circulation in the absence and presence of wind turbines, a model validation exercise was performed using model output in the absence of turbines. Sea surface temperature data were obtained over the 1988-2000 period from the NOAA 1/4° Daily

Optimum Interpolation Sea Surface Temperature (OISST). This product is a long term climate data record that incorporates observations from different platforms (satellites, ships, buoys, and Argo floats) into a regular global grid. The NOAA High Resolution SST data is provided by the NOAA/OAR/ESRL PSL, Boulder, Colorado, USA, from the web site https://psl.noaa.gov/data/gridded/data.noaa.oisst.v2.highres.html#detail .

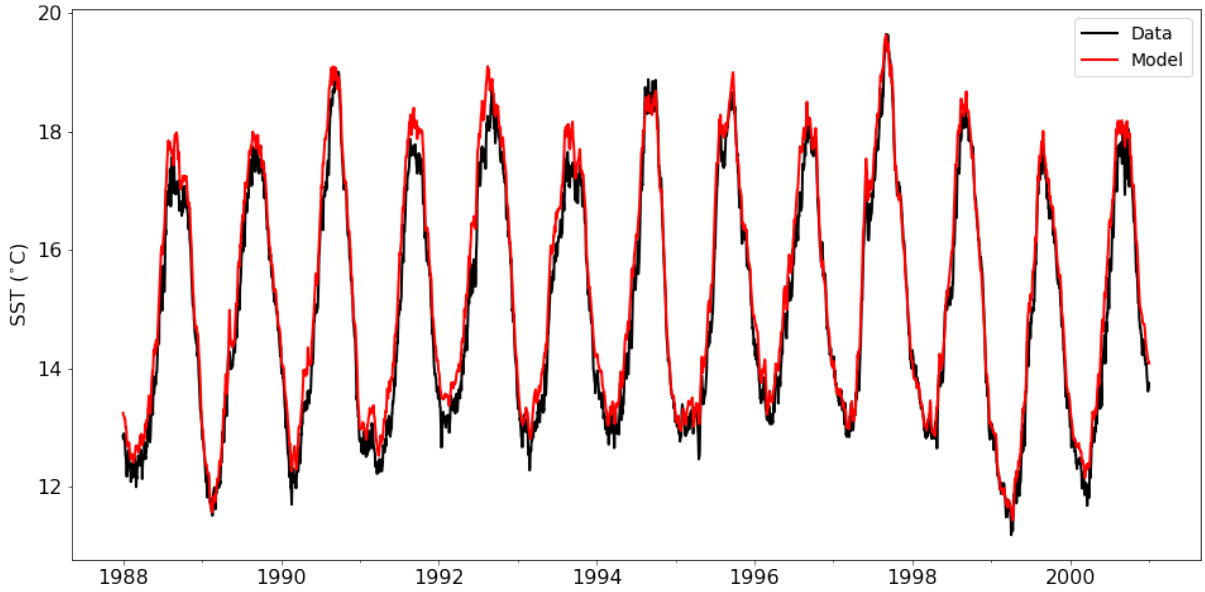

Figure 11. Domain-averaged WC12 sea surface temperatures, compared to those from the NOAA 1/4° SST product.

Domain-averaged sea surface temperatures for the WC12 domain are compared against the NOAA SST data in Figure 11. An excellent reproduction of sea surface temperatures is observed. Biases, when present, tend to trend somewhat warm, with a maximum difference of approximately 0.5 °C in 1992. Figure 11 also shows climatological variability such as those associated with warm surface waters during El Nino years (1996-1997) and cooler waters associated with La Nina years (1989-1999).

Figure 12 compares WC15 seasonal sea surface temperatures against the NOAA SST data. The model is seen to accurately reproduce large scale temperature gradients such as the North-South gradient between the Oregon Coast and Point Conception, and the warming of surface waters inside the Southern California Bight. The model is also seen to capture the occurrence of upwelling in the spring, with the correct placement of upwelling hotspots, such as those near Cape Blanco (43°N) and Cape Mendocino (40.5°N). Nevertheless, the modest warm bias is seen to persist through the seasons, in contrast to model-data differences observed by Veneziani et al. (2009), and Broquet et al. (2009). This difference is attributed to use of a different wind forcing (i.e. WRF) in this study, in contrast to the use of the Coupled Ocean/Atmosphere Mesoscale Prediction System (COAMPS) atmospheric products by the above authors. Nonetheless, the absolute bias in sea surface temperatures is lower than that found by the above

authors. In particular, Veneziani et al. (2009) found an approximately 2.5°C warm bias offshore of Washington, Cape Blanco, and Cape Mendocino in September, which appears to be largely absent in this study. These comparisons lend confidence that the model reproduces key circulation features with adequate skill to be applied to the question of evaluating potential changes in upwelling due to the installation of offshore wind farms.

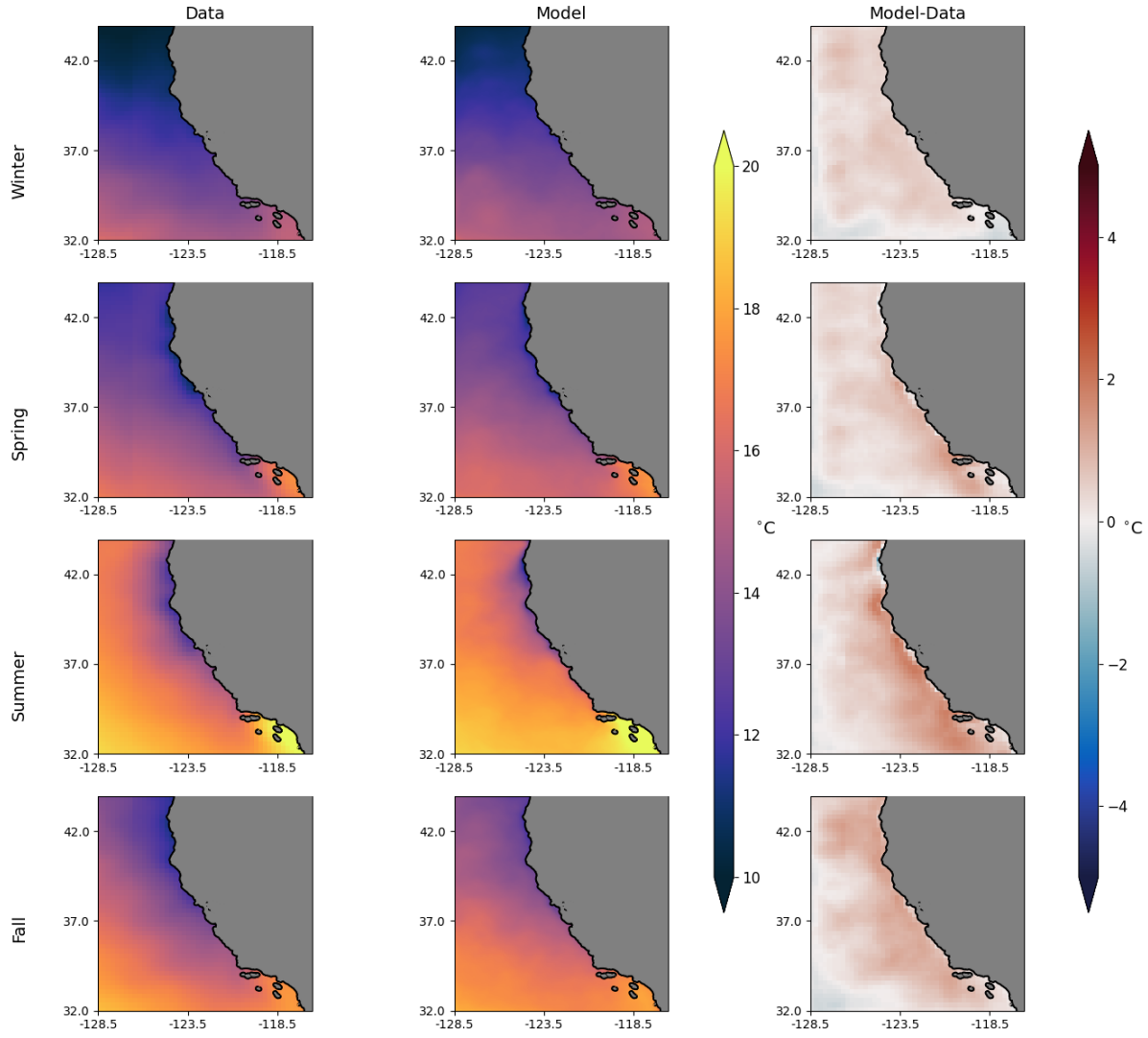

Figure 12. Seasonal comparison of WC15 sea surface temperatures against those from the NOAA 1/4° SST product.

Having established adequate skill in reproducing the timing and location of circulation features, comparisons are made in the absence and presence of wind farms within the Humboldt, Morro Bay, and Diablo Canyon call areas. These comparisons only account for the effect of the turbines on atmospheric circulation and the resulting changes in forcing to the ocean surface. They do

not account for potential changes in circulation due to the physical presence of wind turbines in the ocean, and the resulting wake-induced mixing around multiple wind turbines (Schultze et al., 2020).

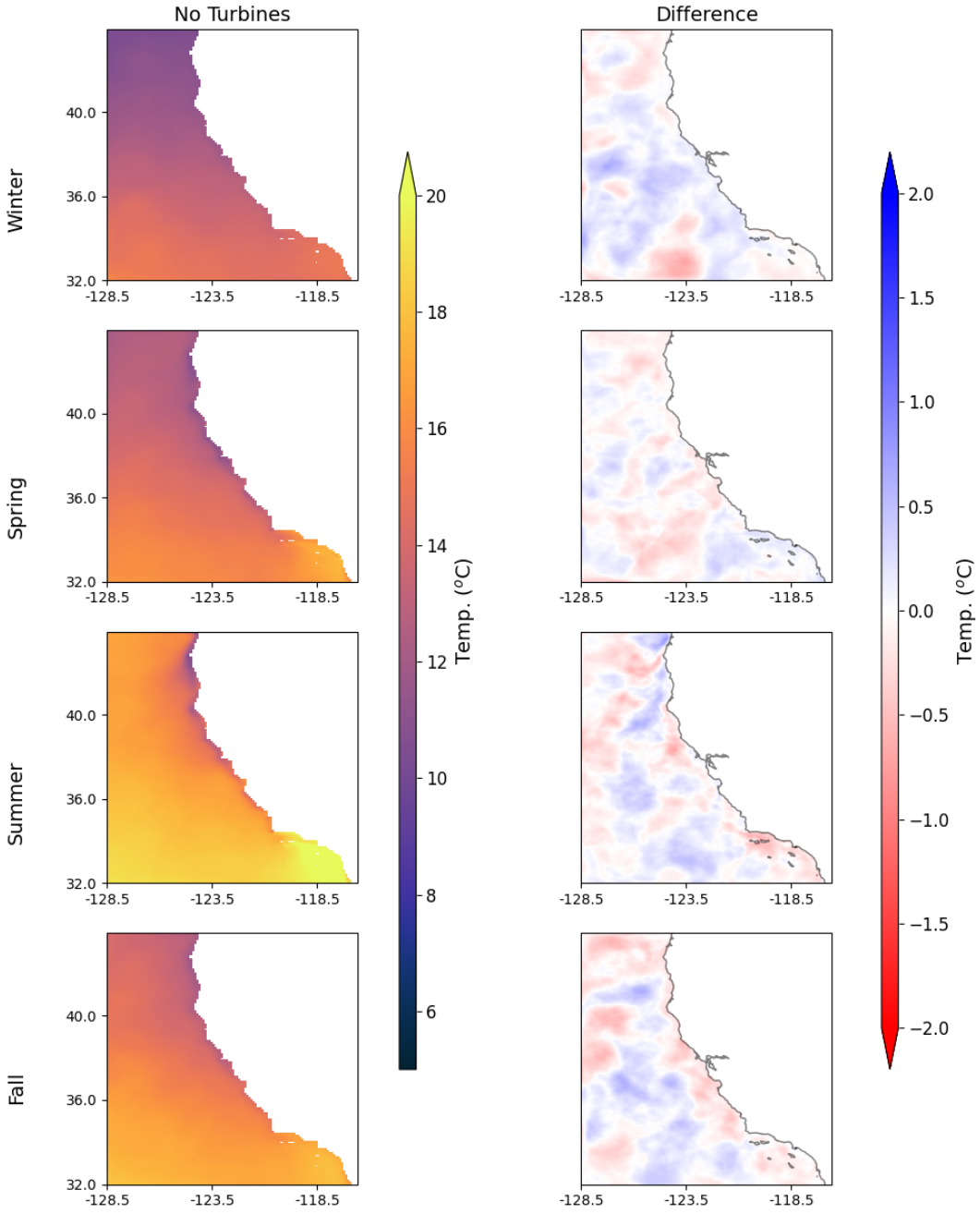

Figure 13. Seasonal changes in sea surface temperature in the presence of offshore wind farms. (Left) Seasonal SST without wind turbines, (right) SST differences = without - with turbines.

Seasonal changes in SST are shown in Figure 13, averaged over the period 1988-2000. Changes are modest and primarily trend towards modest cooling in the winter following the

introduction of turbines. A warming pattern (relative to the case without turbines) begins to establish in the spring, particularly in the immediate vicinity of the Humboldt and Morro Bay/Diablo Canyon call areas. This trend proceeds to propagate southward through the fall and winter, consistent with the development of an equatorward coastal upwelling jet (Lynn et al., 2003). Interestingly, while wind speeds are only modified in the vicinity of the call areas (Figure 7), the resulting changes in circulation are observed to propagate throughout the model domain. Of course, not all of these changes necessitate an impact to coastal upwelling and ecosystem productivity.

Since upwelling is characterized by the tilting of isopycnal (constant density) surfaces, it is particularly insightful to examine density surfaces to evaluate changes in upwelling. Figure 14 shows surface density averaged over the model run period. As an illustrative example, the contour for the 25 kg/m^3 density surface (relative to a background density of 1000 kg/m^3) reveals that while waters at this density are present in the nearshore region near Morro Bay/Diablo Canyon in the absence of wind turbines, these denser waters are largely absent following the installation of wind farms. The difference plot for surface density further shows a general trend towards the presence of less dense waters along the coast, indicating reduced upwelling.

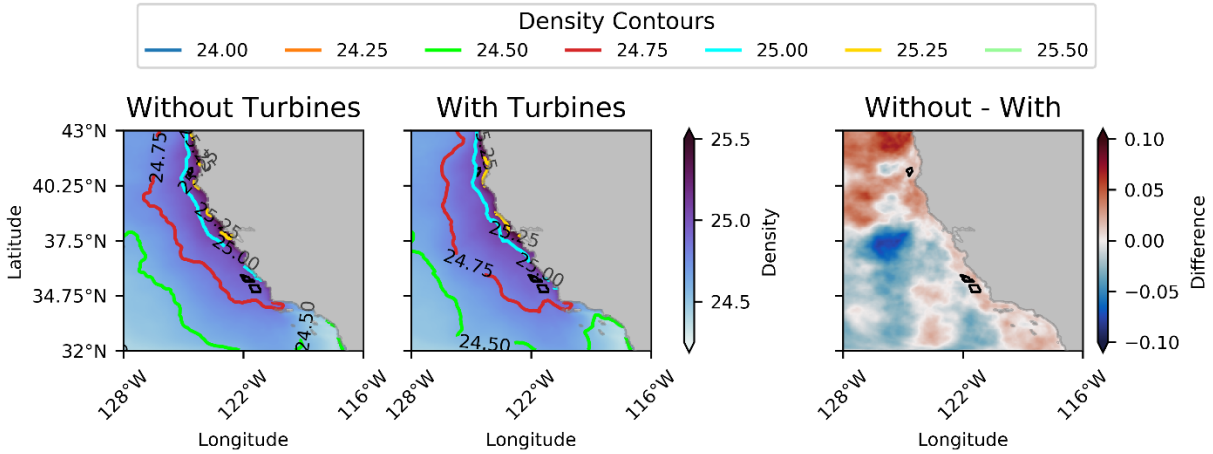

Figure 14. Average density at the ocean surface. (Left) without turbines, (middle) with turbines, and (right), density difference=without-with turbines, over the 1988-2000 time period.

The depth structure of density is examined next, with an eye towards shedding further light on changes to upwelling. Figure 15 shows the seasonal evolution of the density structure in the upper 500 m at 34.5°N, located south of the Diablo Canyon call area, and north of Point Conception. Upwelling-induced tilting of isopycnals is evident in the contours for the 25 kg/m^3 and 26 kg/m^3 density contours. Relaxation of isopycnal tilting is evident offshore of 122°W, and is most pronounced in the spring. Nearshore (east of 121.75°W) reduction in upwelling is evident in a narrow band along the coast, with the deepest reduction in the spring with lessened impacts in the summer and fall. No noticeable reduction in upwelling is observed in the winter. Density changes are observed to exhibit a banded pattern consistent with canonical two-cell convergence and divergence around upwelling fronts (Suginohara, 1977).

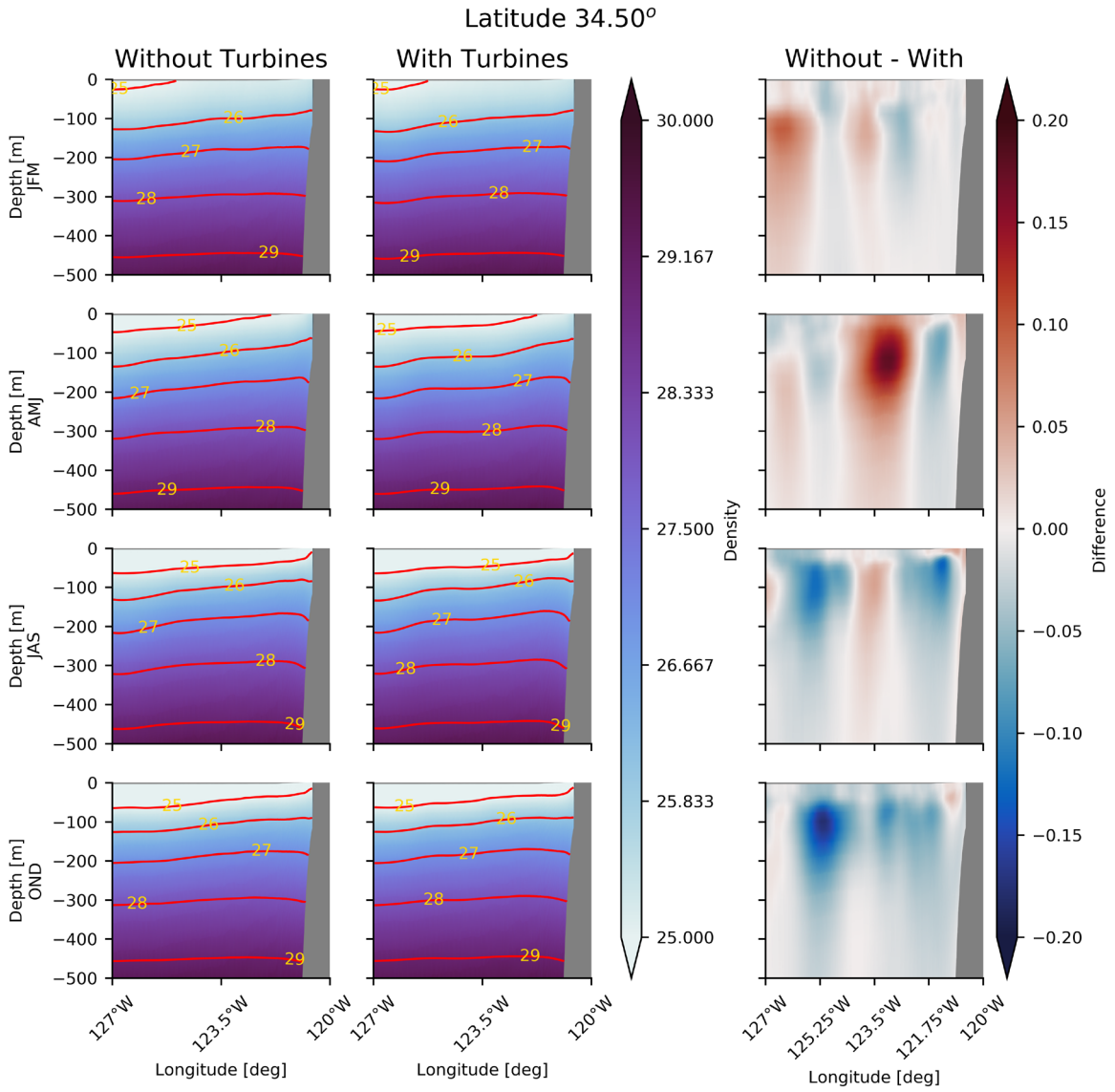

Figure 15. Vertical section of seasonal density at 34.5°N (located south of the Diablo Canyon call area). Shown are seasonal sections, (left) without turbines, (right) with turbines, and (middle) difference = without turbine - with turbines.

3.3 UPWELLING METRICS

The model run in the absence of turbines produces upwelling patterns consistent with those previously documented for the U.S. west coast (Figure 16). Upwelling is strongest in the spring/summer, with peak values occurring later in the year at higher latitudes. The strongest seasonal upwelling occurs in the vicinity of Cape Mendocino (38-40°N), with a secondary peak off central California, offshore of Morro Bay (~35°N). CUTI and BEUTI exhibit similar seasonal and spatial variability, indicating that for the mean patterns, vertical nitrate flux closely tracks upwelling strength.

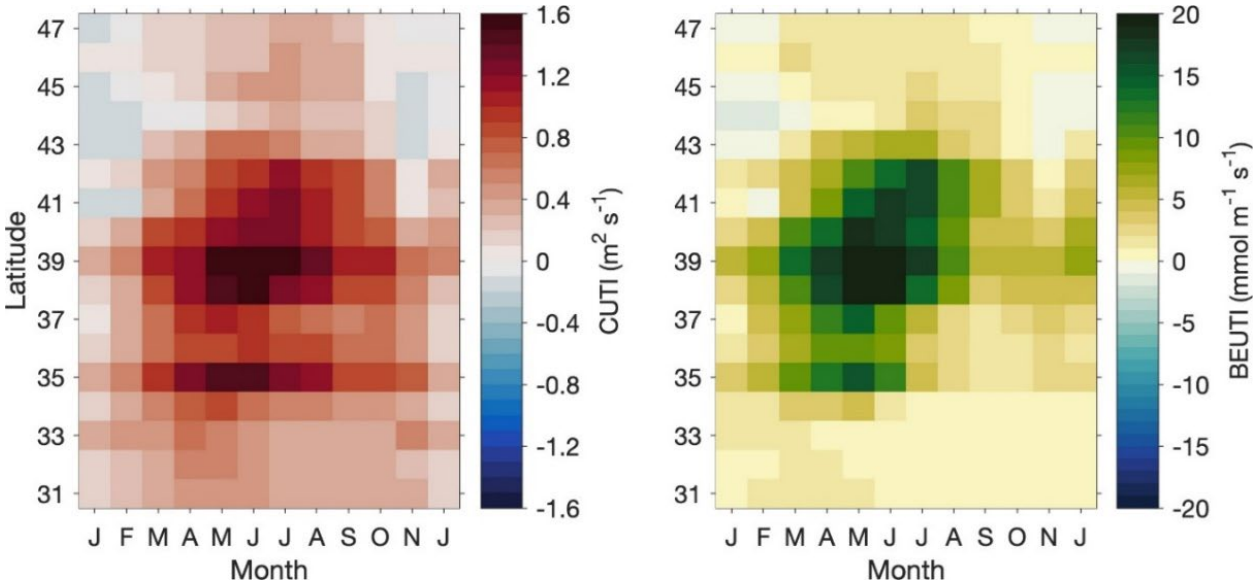

Figure 16. Seasonal and latitudinal variability in CUTI and BEUTI (baseline). For CUTI (left) and BEUTI (right), monthly climatologies are shown as a function of latitude.

Comparing upwelling indices in the absence of turbines to the case with the wind field altered by turbines, a pronounced change is observed at 35°N, with minor effects elsewhere (Figure 17). At 35°N, introducing wind turbines reduces CUTI and BEUTI by 10% and 15%, respectively – changes that fall outside of the interannual variability of each index. The fact that nitrate flux (BEUTI) is decreased more than upwelling transport (CUTI) indicates that the wind farm at 35°N reduces not just upwelling strength, but also the nitrate content of upwelled waters due to the inverse correlation between temperature and nitrate concentration.

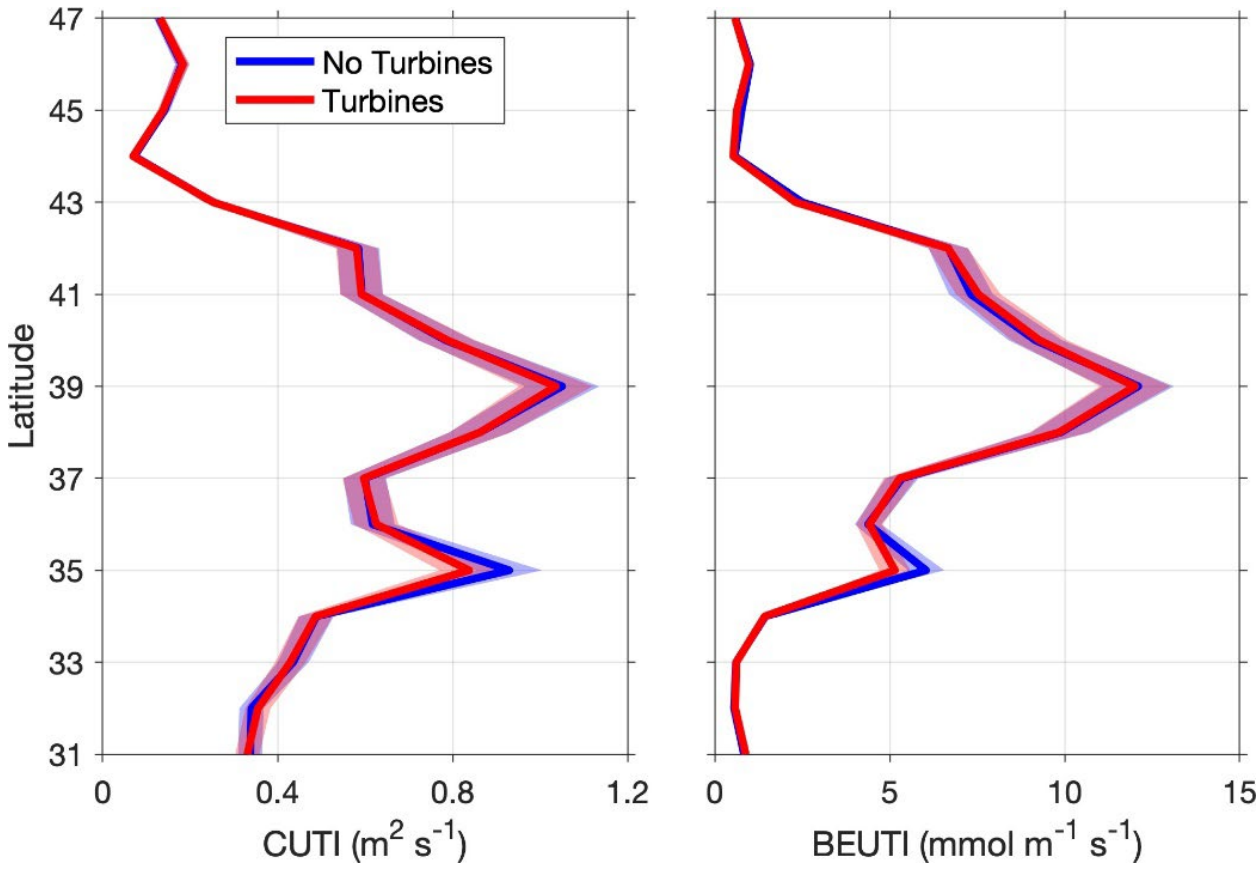

Figure 17. Long-term (1988-2000) mean of CUTI (left) and BEUTI (right) for simulations with (red) and without (blue) wind turbines. Shading indicates +/- one standard deviation of annual means.

Over the 13-year span of the model simulations, there is considerable variability in CUTI and BEUTI at 35°N (Figure 18). Of particular note are years when upwelling was strongly inhibited by El Niño events (1992 and 1998). Both CUTI and BEUTI are consistently lower at 35°N in the case with wind turbines than the case without, but for individual years the difference between the two cases can be enhanced or suppressed. The reasons for those fluctuations are yet to be explored.

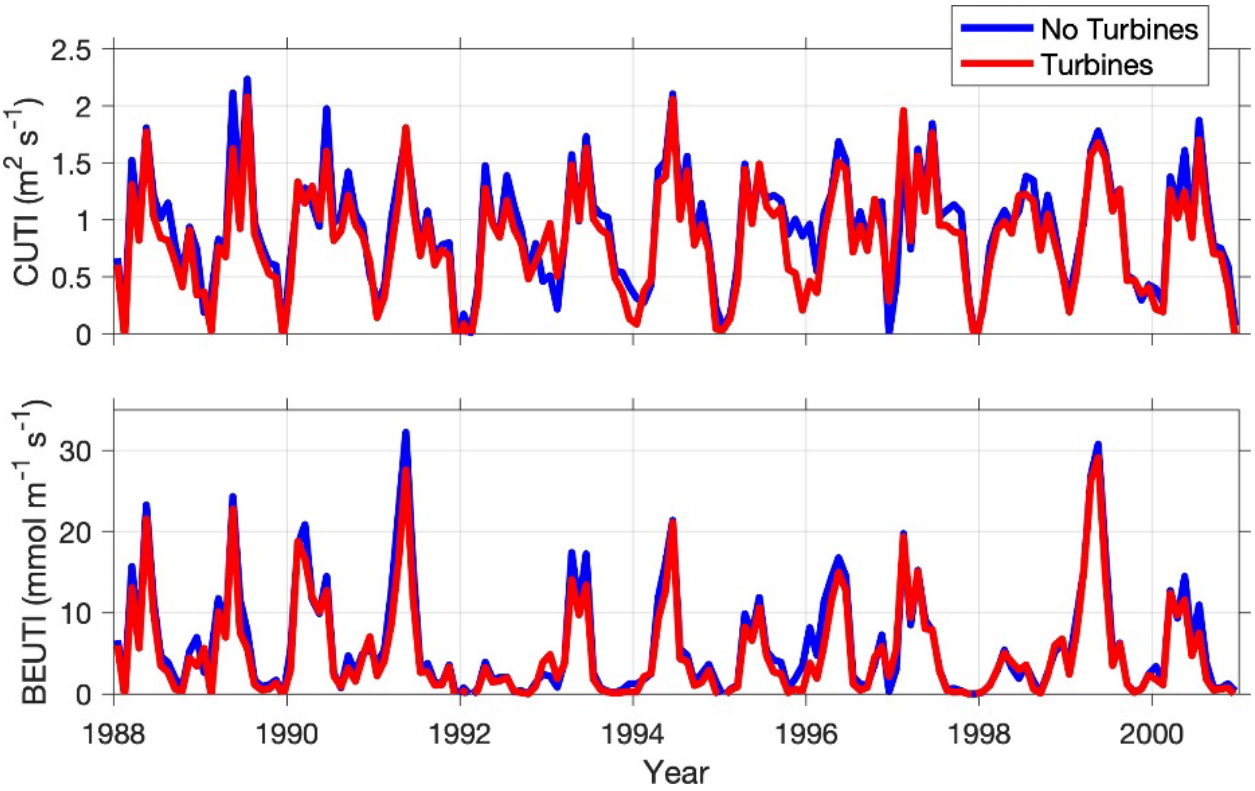

Figure 18. Monthly time series of CUTI (top) and BEUTI (bottom) for simulations with (red) and without (blue) wind turbines. Time series are shown for 35˚N, where the impact of wind farms on upwelling is greatest.

Finally, while upwelling is strongest close to the coast, it can in some cases extend far offshore (100 km or more), so upwelling indices are calculated over wider coastal bands to capture any cross-shore differences in the effects of wind turbines on upwelling (Figure 19). As the offshore extent of upwelling indices is increased, there is a change in the pattern of upwelling modification near Morro Bay. Farther offshore, turbine-induced decreases in upwelling are shifted to the north (from ~35°N to ~36°N), while upwelling appears to be enhanced south of Point Conception (~34°N).

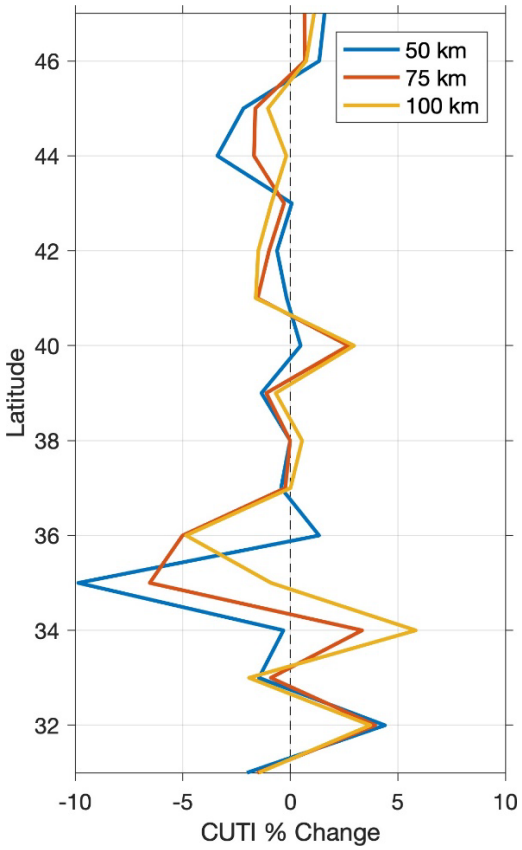

Figure 19. Percentage change in CUTI due to wind turbines. Colored lines show changes as a function of latitude for indices calculated over three different cross-shore distances (50 km, 75 km, 100 km, corresponding to the contour lines in Fig. 6).

4 DISCUSSION AND CONCLUSIONS

The length and location of California's coastline along the eastern boundary of the Pacific Ocean results in a tremendous wind energy resource that is characterized by nearly year-round northwesterly winds. As promising as this wind field is as a source of offshore wind energy, it also supports a thriving marine ecosystem through wind-induced coastal upwelling of cooler, nutrient-rich waters. The development of offshore wind in California will therefore need to consider the potential implications of offshore wind energy extraction on the strength of coastal upwelling.

Here, a first step towards addressing this concern is taken through the application of a one-way coupled atmosphere-ocean model to evaluate the potential effects of wind turbine arrays on atmospheric parameters of relevance as forcing parameters to an ocean circulation model. The wind field parameterization within the atmospheric model (WRF-WFP) was applied to a full build-out of wind turbines at the Humboldt, Morro Bay, and Diablo Canyon call areas. This method has been previously applied to evaluate the effects of wind farms on atmospheric circulation at a number of onshore and offshore geographic locations (Roy &Traiteur [2010], Lee & Lundquist [2017], Huang & Hall [2015], Duin [2019]), with the Huang & Hall (2015) study being particularly relevant to this work due to its study site located offshore of Bodega Bay, California. The atmospheric model was run with boundary conditions, physics parameterizations and turbine parameters (hub heights, rotor diameter, thrust coefficients) that are identical to the previously validated model that was reported in Optis et al. (2020).

The WRF-WFP model was run without and with simulated wind turbines and evaluated for a period of 13 years (1988-2000). A seasonal pattern in wind stress reduction was observed, with the reduction being most pronounced during the spring and summer months (April-September) when wind speeds were strongest. Changes to wind speeds and other atmospheric forcing fields were considerably more pronounced for the Morro Bay/Diablo Canyon call areas, relative to the Humboldt call area. This is a reasonable result given that the size and number of turbines for Humboldt is about 4 times smaller than the combined Morro Bay/Diablo Canyon sites. Wind speed reductions were observed in excess of 1 m/s, or roughly 5% of maximum wind speeds, with the Morro Bay wake that extends past the Channel Islands. The wind speed deficit is qualitatively similar to measured offshore wind farm wakes by Cañadillas (2020). The areal extents of the wakes are on the order of several times the modified Rossby radii of deformation (De Szoeke & Richman, 1984), and are on the order of spatial scales to affect rotational processes such as coastal upwelling.

WRF fields without and with turbines for the 13-year model run were used as forcing fields to drive a nested ocean model (ROMS) at 10 km and 3 km resolutions. Prior to evaluating changes in ocean circulation and upwelling following the introduction of wind turbines, a model validation exercise was performed. The model was seen to appropriately capture spatial

features such as the North-South temperature gradient between the Oregon Coast and Point Conception, the warming of surface waters inside the Southern California Bight, and the locations of upwelling hotspots, such as those near Cape Blanco (43°N)and Cape Mendocino (40.5°N). The model is also seen to reproduce temporal features such as the onset of upwelling in the spring, it's continued evolution through the summer, followed by a return to neutral/downwelling conditions over the winter. The model is seen to exhibit a slight warm bias, in contrast to generally cool biases observed by Veneziani et al. (2009), and Broquet et al. (2009). Nonetheless, the absolute bias in sea surface temperatures is lower than that found by the above authors. For example, Veneziani et al. (2009) found an approximately 2.5°C warm bias offshore of Washington, Cape Blanco and Cape Mendocino in September, which appears to be largely absent in this study.

The potential effects of offshore wind farms on circulation were evaluated in terms of changes in sea surface temperature, density structure, mixed-layer depth, vertical velocities, and upwelling metrics that describe volume transport and nutrient flux into the coastal zone. The reduction of wind stress is seen to cause a warming of coastal sea surface temperatures starting in the spring, and evolving into the fall. While changes in sea surface temperature show less of a bias towards coastal warming in the winter, changes are widespread across the model domain, suggesting the offshore propagation of coastal wind-driven upwelling processes (and therefore changes to the above). Strub & James (2000), using altimeter measurements, found a similar offshore propagation of the equatorward coastal upwelling jet that develops in the spring and summer, into deeper offshore waters in the fall and winter. In the context of wind farm development, these results indicate that changes in circulation, induced in relatively small regions can propagate several hundred kilometers offshore. While these changes may not necessarily impact ecosystem productivity, functions and services, they are nevertheless present and may potentially warrant further investigation.

The three-dimensional density structure was examined in the absence and presence of wind turbines, with a focus on the upper 500 m of the water column, within 300 – 600 km of the coast. Surface density maps indicate a change in the location of the upwelling front, with a shoreward displacement of the 25 kg/m^3 isopycnal contour, indicative of a reduction in the slope of the upwelling front due to weakened upwelling. Paskyabi (2015) observed a similar shoreward displacement of the upwelling front in an idealized two-dimensional study of the effects of wind farm wakes on stratification and coastal upwelling. Interestingly, the depth structure of density changes reveals changes in both the nearshore (<50 km offshore) and further offshore (100-200 km). With the onset of upwelling in the spring, the reduction of wind stress in the presence of turbines results in a reduction of the slope of the 26 kg/m^3 isopycnal contour east of 121.75° W. Changes in the density structure are deepest in the spring, but shallower and of greater magnitude in the summer due to increased stratification of the upper water column in the summer that can tend to suppress upwelling-induced tilting of isopycnals (Jacox et al., 2015). As the seasons transition into the fall, the reduced stratification reverts back to greater density differences at depth, albeit with a lower magnitude. While the nearshore effects are of

particular importance to nutrient delivery and phytoplankton production, the offshore changes in density structure, particularly during the spring, are most prominent. The offshore changes are hypothesized to be a result of wind stress curl driven divergence/convergence, due to the horizontal shear in wind speeds induced by wind farm wake effects. This hypothesis is motivated by prior findings by Brostrom (2008), who investigated the effect of wind stress shear due to wind farm wakes and found changes to the pycnocline structure, with the occurrence of curl-driven upwelling and downwelling on either side of the wind wake region. The calculation of upwelling metrics over a wide offshore region (100 km as opposed to the operationally used extent of 75 km) appear to indicate a further enhanced impact to volume transport in the presence of turbines, further suggesting that wind stress curl-driven processes might require further investigation.

An initial step towards understanding the impact of modeled changes in physical upwelling circulation to ecosystem impacts was undertaken by computing upwelling indices that have been found to be closely related to ecosystem production (Bakun, 1973 and 1975). The computed upwelling indices consist of two products that are routinely produced at NOAA's Southwest Fisheries Science Center: the Coastal Upwelling Transport Index (CUTI), which estimates vertical volume transport, and the Biologically Effective Upwelling Transport Index (BEUTI), which estimates vertical nitrate flux. Monthly climatological variability in CUTI and BEUTI were verified to align with those previously reported (Jacox et al., 2018), with peaks in upwelling occurring in the spring and summer, with the peaks occurring later in the year at higher latitudes. The strong correlation observed between the CUTI and BEUTI estimates indicates that the nitrate flux into the euphotic zone closely tracks the volume transport index. Latitudinal variability in the upwelling indices shows peaks in upwelling strength near Cape Mendocino (39°N) and near the Morro Bay call area (35°N). These peaks in upwelling strength are directly related to the strength of climatological wind speeds that have been observed to intensity offshore of Cape Mendocino and Point Conception (Fiechter et al., 2018, and Optis et al., 2020). Little change in the upwelling indices were observed at the Humboldt call area. However, at 35°N, the presence of wind turbines reduces CUTI and BEUTI by 10% and 15%, respectively – changes that fall outside of the interannual variability of each index. The fact that nitrate flux (BEUTI) is decreased more than upwelling transport (CUTI) indicates that wind turbines at 35°N reduce not just upwelling strength, but also the nitrate content of upwelled waters. While considerable inter-annual variability in CUTI and BEUTI was observed at 35°N, there remained the consistent pattern of reduction in upwelling in the presence of wind farms. Notable exceptions to this observation are years when upwelling was strongly inhibited by El Niño events (1992 and 1998). This difference could potentially be due to enhanced stratification and accumulation of nutrients below the euphotic zone during El Niño events (Sydeman et al., 2014).

It should be stressed that this study only examined the effect of wind stress reductions on the physical oceanographic circulation. Therefore, no conclusions on ecosystem impacts can be drawn from the modeled physical changes. Evaluation of ecosystem effects requires the

application of coupled physical-biological models, which is currently beyond the scope of this preliminary study.

In summary, this study shows that the use of coupled atmosphere-ocean models can help quantify potential changes to upwelling circulation induced by the presence of wind turbines. The use of nested domains for the atmosphere and ocean models allow for the resolution of processes on the scale of the wind farm call areas. Changes in wind stress were found to be largest inside the wind farm call areas, though wake effects were seem to persist in the lee of the wind farms. Changes in ocean circulation were described via changes in sea surface temperature and the underlying density structure. When cast in terms of upwelling metrics, a 10-15% change was inferred in upwelled volume transport and resulting nutrient flux to the euphotic zone. The impact of these changes on the phytoplankton productivity, while expected to be present, is currently unknown and beyond the scope of this study.

As with all modeling efforts, uncertainties are undoubtedly present. These include discretization effects (i.e. the finite resolution of the atmosphere and ocean model) that fail to resolve finer scale turbulence processes and the cascading effects of these on larger scale processes. The use of a one-way coupled model (i.e. no ocean feedback on the lower atmospheric boundary layer) neglects well-known effects of upper ocean dynamics on the lower atmospheric. The use of a fully-coupled model is, however, still an active area of research and not suitable for a study focused on a specific question such as this study. Further, the use of identical modeling approaches to evaluate the effects of wind farms on upwelling has the advantage of yielding comparative insights given that identical uncertainties exist in both the control run (no turbines) and in the modified state estimates (turbines present).

Future areas of investigation will include a sensitivity study of the effect of varying turbine parameters (hub heights, rotor diameter, number, and placement of turbines in a call area), and the resulting effects on upwelling. Impacts to upwelling in the context of larger basin-scale processes such as El Niño Southern Oscillation (ENSO) will also be evaluated in the coming months. Other areas of investigation include a more in-depth look at the wind-stress curl-driven upwelling and potential changes to this process in the presence of wind farms. Other potential efforts could include studies to evaluate the impacts on higher trophic levels, including fisheries and socio-economic impacts, links to life histories of megafauna (Oestrich et al., 2021), and variability in upwelling effects in the face of climate change.

5 REFERENCES

Bakun, A. 1973. Coastal upwelling indices, West Coast of North America, 1946–71. NOAA Technical Report NMFS SSRF-671. U.S. Department of Commerce, National Oceanic and Atmospheric Administration, National Marine Fisheries Service, Seattle, WA.

Bakun, A. 1975. Daily and weekly upwelling indices, West Coast of North America. NOAA Technical Report 16.

Beiter, P., Musial, W., Duffy, P., Cooperman, A., Shields, M., Heimiller, D. and Optis, M., 2020. *The Cost of Floating Offshore Wind Energy in California Between 2019 and 2032* (No. NREL/TP-5000-77384; BOEM-2020-48). National Renewable Energy Lab. (NREL), Golden, CO (United States).

Bograd, S.J., Checkley Jr, D.A., and Wooster, W.S., 2003. CalCOFI: A half century of physical, chemical, and biological research in the California Current System. *Deep Sea Research Part II: Topical Studies in Oceanography* 50(14–16):2349–2353.

Broquet, G., Edwards, C.A., Moore, A.M., Powell, B.S., Veneziani, M., and Doyle, J.D., 2009. Application of 4D-Variational data assimilation to the California Current System. *Dynamics of Atmospheres and Oceans* 48(1–3):69–92.

Brostrom, G., 2008. On the influence of large wind farms on the upper ocean circulation. *Journal of Marine Systems* 74:585–591.

Budgell, W.P., 2005: Numerical simulation of ice-ocean variability in the Barents Sea region, Ocean Dynamics, DOI 10.1007/s10236-005-0008-3.

Cañadillas, B., Foreman, R., Barth, V., Siedersleben, S., Lampert, A., Platis, A., Djath, B., Schulz-Stellenfleth, J., Bange, J., Emeis, S. and Neumann, T., 2020. Offshore wind farm wake recovery: Airborne measurements and its representation in engineering models. *Wind Energy*, *23*(5), pp.1249-1265.

Carton, J. A., Chepurin, G., & Cao, X., 2000. A Simple Ocean Data Assimilation analysis of the global upper ocean 1950-1995. Part 2: Results. *Journal of Physical Oceanography*, 30(2), 311–326. https://doi.org/10.1175/1520-0485(2000)030%3C0311:ASODAA%3E2.0.CO;2

Checkley Jr, D.M. and Barth, J.A., 2009. Patterns and processes in the California Current System. *Progress in Oceanography* 83:49–64.

Churchfield, M.J., Lee, S., Michalakes, J. and Moriarty, P.J., 2012. A numerical study of the effects of atmospheric and wake turbulence on wind turbine dynamics. *Journal of turbulence*, (13), p.N14.

De Szoeke, R.A. and Richman, J.G., 1984. On wind-driven mixed layers with strong horizontal gradients—A theory with application to coastal upwelling. *Journal of physical oceanography*, *14*(2), pp.364-377.

Di Lorenzo, E., 2003: Seasonal dynamics of the surface circulation in the southern California Current System, Deep-Sea Res., Part II, 50, 2371-2388.

Dinniman, M.S., Klinck, J.M. and Smith Jr, W.O., 2003. Cross-shelf exchange in a model of the Ross Sea circulation and biogeochemistry. *Deep Sea Research Part II: Topical Studies in Oceanography*, *50*(22-26), pp.3103-3120.

Duin, M., 2019. Effect of wind farms at the North Sea on meteorological conditions in the Netherlands. M.S. thesis.

Eriksson, O., Lindvall, J., Breton, S.P. and Ivanell, S., 2015, June. Wake downstream of the Lillgrund wind farm-A Comparison between LES using the actuator disc method and a Wind farm Parametrization in WRF. In *Journal of physics: Conference series* (Vol. 625, No. 1, p. 012028). IOP Publishing.

Fiechter, J., Edwards, C.A. and Moore, A.M., 2018. Wind, circulation, and topographic effects on alongshore phytoplankton variability in the California Current. *Geophysical Research Letters*, *45*(7), pp.3238-3245.

Fitch, A.C., Olson, J.B., Lundquist, J.K., Dudhia, J., Gupta, A.K., Michalakes, J. and Barstad, I., 2012. Local and mesoscale impacts of wind farms as parameterized in a mesoscale NWP model. *Monthly Weather Review*, *140*(9), pp.3017-3038.

Goebel, N.L., Edwards, C.A., Zehr, J.P. and Follows, M.J., 2010. An emergent community ecosystem model applied to the California Current System. *Journal of Marine Systems*, *83*(3-4), pp.221-241.

Haidvogel, D.B., Arango, H.G., Hedstrom, K., Beckmann, A., Malanotte-Rizzoli, P. and Shchepetkin, A.F., 2000. Model evaluation experiments in the North Atlantic Basin: simulations in nonlinear terrain-following coordinates. *Dynamics of atmospheres and oceans*, *32*(3-4), pp.239-281.

Hersbach, H., Bell, B., Berrisford, P., Biavati, G., Horányi, A., Muñoz Sabater, J., Nicolas, J., Peubey, C., Radu, R., Rozum, I. and Schepers, D., 2018. ERA5 hourly data on single levels from 1979 to present. *Copernicus Climate Change Service (C3S) Climate Data Store (CDS)*, *10*.

Huang, H.Y., and Hall, A., 2015. Preliminary assessment of offshore wind development impacts on marine ecosystems. CEC-500-2016-023. Prepared for California Energy Commission. UCLA Department of Atmospheric and Oceanic Sciences, Los Angeles, CA. March, 2015.

Jacox, M.G., Bograd, S.J., Hazen, E.L. and Fiechter, J., 2015. Sensitivity of the California Current nutrient supply to wind, heat, and remote ocean forcing. *Geophysical Research Letters*, *42*(14), pp.5950-5957.

Jacox, M.G., Hazen, E.L. and Bograd, S.J., 2016. Optimal environmental conditions and anomalous ecosystem responses: Constraining bottom-up controls of phytoplankton biomass in the California Current System. *Scientific Reports*, *6*(1), pp.1-12.

Jacox, M.G., Edwards, C.A., Hazen, E.L. and Bograd, S.J., 2018. Coastal upwelling revisited: Ekman, Bakun, and improved upwelling indices for the U.S. West Coast. *Journal of Geophysical Research: Oceans*, *123*(10), pp.7332-7350.

Jiménez, P.A., Navarro, J., Palomares, A.M. and Dudhia, J., 2015. Mesoscale modeling of offshore wind turbine wakes at the wind farm resolving scale: A composite-based analysis with the Weather Research and Forecasting model over Horns Rev. *Wind Energy*, *18*(3), pp.559-566.

Lee, J.C. and Lundquist, J.K., 2017. Evaluation of the wind farm parameterization in the Weather Research and Forecasting model (version 3.8. 1) with meteorological and turbine power data. *Geoscientific Model Development*, *10*(11), pp.4229-4244.

Lowe, A. B. (2020). Modeling of coastal processes and Lagrangian transport around the Monterey Peninsula. UC Santa Cruz. ProQuest ID: Lowe_ucsc_0036E_12120. Merritt ID: ark:/13030/m5tj41jf. Retrieved from https://escholarship.org/uc/item/4tf8p3r9.

Lynn, R. J., Bograd, S. J., Chereskin, T. K., and Huyer, A. (2003), Seasonal renewal of the California Current: The spring transition off California, *J. Geophys. Res.*, 108, 3279, doi:10.1029/2003JC001787, C8.

Marchesiello, P., McWilliams, J.C. and Shchepetkin, A., 2003. Equilibrium structure and dynamics of the California Current System. *Journal of physical Oceanography*, *33*(4), pp.753-783.

Musial, W., Beiter, P., Tegen, S. and Smith, A., 2016. *Potential offshore wind energy areas in California: An assessment of locations, technology, and costs* (No. NREL/TP-5000-67414). National Renewable Energy Lab.(NREL), Golden, CO (United States).

Neveu, E., Moore, A.M., Edwards, C.A., Fiechter, J., Drake, P., Crawford, W.J., Jacox, M.G. and Nuss, E., 2016. An historical analysis of the California Current circulation using ROMS 4D-Var: System configuration and diagnostics. *Ocean Modelling*, *99*, pp.133-151.

NMFS. 2018. Fisheries Economics of the United States 2016. Economics and Sociocultural Status and Trends Series. NOAA Technical Memorandum NMFS-F/SPO-187A. U.S. Department of Commerce, National Oceanic and Atmospheric Administration, National Marine Fisheries Service. December.

Oestreich, W., Abrahms, B., McKenna, M., Goldbogen, J., Crowder, L. and Ryan, J., 2021. Acoustic signature reveals blue whales tune life history transitions to oceanographic conditions. Paskyabi, M.B., and I. Fer. 2012. Upper ocean response to large wind farm effect in the presence of surface gravity waves. *Energy Procedia* 24:245–254.

Optis, M., Rybchuk, O., Bodini, N., Rossol, M. and Musial, W., 2020. *2020 Offshore Wind Resource Assessment for the California Pacific Outer Continental Shelf* (No. NREL/TP-5000-77642). National Renewable Energy Lab.(NREL), Golden, CO (United States).

Paskyabi, M.B. 2015. Offshore wind farm wake effect on stratification and coastal upwelling. *Energy Procedia* 80:131–140.

Peliz, Á., Dubert, J., Haidvogel, D.B. and Le Cann, B., 2003. Generation and unstable evolution of a density-driven eastern poleward current: The Iberian poleward current. *Journal of Geophysical Research: Oceans*, *108*(C8).

Raghukumar, K., Edwards, C.A., Goebel, N.L., Broquet, G., Veneziani, M., Moore, A.M. and Zehr, J.P., 2015. Impact of assimilating physical oceanographic data on modeled ecosystem dynamics in the California Current System. *Progress in Oceanography*, *138*, pp.546-558.

Roy, S.B. and Traiteur, J.J., 2010. Impacts of wind farms on surface air temperatures. *Proceedings of the National Academy of Sciences*, *107*(42), pp.17899-17904.

Rykaczewski, R.R. and Checkley, D.M., 2008. Influence of ocean winds on the pelagic ecosystem in upwelling regions. *Proceedings of the National Academy of Sciences*, *105*(6), pp.1965-1970.

Shchepetkin, A.F. and McWilliams, J.C., 2005. The regional oceanic modeling system (ROMS): a split-explicit, free-surface, topography-following-coordinate oceanic model. *Ocean modelling*, *9*(4), pp.347-404.

Schultze, L.K.P., Merckelbach, L.M., Horstmann, J., Raasch, S. and Carpenter, J.R., 2020. Increased mixing and turbulence in the wake of offshore wind farm foundations. *Journal of Geophysical Research: Oceans*, *125*(8), p.e2019JC015858.

Severy, M. and Garcia, T., 2020. Description of Study Assumptions. *California North Coast Offshore Wind Studies. Humboldt, CA: Schatz Energy Research Center. schatzcenter. org/pubs/2020-OSW-R1. pdf*.

Strub, P.T. and James, C., 2000. Altimeter-derived variability of surface velocities in the California Current System: 2. Seasonal circulation and eddy statistics. *Deep Sea Research Part II: Topical Studies in Oceanography*, *47*(5-6), pp.831-870.

Suginohara, N., 1977. Upwelling front and two-cell circulation. *Journal of the Oceanographical Society of Japan*, *33*(3), pp.115-130.

Sydeman, W.J., García-Reyes, M., Schoeman, D.S., Rykaczewski, R.R., Thompson, S.A., Black, B.A. and Bograd, S.J., 2014. Climate change and wind intensification in coastal upwelling ecosystems. *Science*, *345*(6192), pp.77-80.

Tomaszewski, J.M. and Lundquist, J.K., 2020. Simulated wind farm wake sensitivity to configuration choices in the Weather Research and Forecasting model version 3.8. 1. *Geoscientific Model Development*, *13*(6), pp.2645-2662.

Veneziani, M., Edwards, C.A., Doyle, J.D. and Foley, D., 2009. A central California coastal ocean modeling study: 1. Forward model and the influence of realistic versus climatological forcing. *Journal of Geophysical Research: Oceans*, *114*(C4).

Wilkin, J.L., Arango, H.G., Haidvogel, D.B., Lichtenwalner, C.S., Glenn, S.M. and Hedström, K.S., 2005. A regional ocean modeling system for the Long-term Ecosystem Observatory. *Journal of Geophysical Research: Oceans*, *110*(C6).

Wiser, R., Jenni, K., Seel, J., Baker, E., Hand, M., Lantz, E. and Smith, A., 2016. Expert elicitation survey on future wind energy costs. *Nature Energy*, *1*(10), pp.1-8.

Xiu, P., Chai, F., Curchitser, E.N. and Castruccio, F.S., 2018. Future changes in coastal upwelling ecosystems with global warming: The case of the California Current System. *Scientific reports*, *8*(1), pp.1-9.